Geological Magazine

www.cambridge.org/geo

Mafic rocks with back-arc E-MORB affinity from the Chotanagpur Granite Gneiss Complex of India: relicts of a Proterozoic Ophiolite suite

Mansoor Ahmad[1], Abdul Qayoom Paul[2], Priyanka Negi[3], Salim Akhtar[3], Bibhuti Gogoi[4] and Ashima Saikia[3]

[1]Geological Survey of India, Northeastern Region, Shillong, Meghalaya 793003, India; [2]Geological Survey of India, SU: Jammu and Kashmir 190008 India; [3]Department of Geology, University of Delhi, Delhi 110007, India and [4]Department of Geology, Cotton University, Guwahati, Assam 781001, India

Original Article

Cite this article: Ahmad M, Paul AQ, Negi P, Akhtar S, Gogoi B, and Saikia A (2021) Mafic rocks with back-arc E-MORB affinity from the Chotanagpur Granite Gneiss Complex of India: relicts of a Proterozoic Ophiolite suite. *Geological Magazine* **158**: 1527–1542. https://doi.org/10.1017/S0016756821000078

Received: 3 June 2020
Revised: 10 January 2021
Accepted: 19 January 2021
First published online: 18 March 2021

Keywords:
Pillow basalt; Chotanagpur Granite Gneiss Complex; E-MORB; back-arc basalt; supra-subduction zone ophiolite

Author for correspondence: Ashima Saikia, Email: ashima.saikia@gmail.com

Abstract

The Proterozoic Chotanagpur Granite Gneiss Complex (CGGC) at the northern boundary of the Central Indian Tectonic Zone (CITZ) of the eastern Indian shield preserves relics of fossilized oceanic back-arc crust. We describe the field, petrographical and geochemical characteristics of the mafic rocks comprising pillow basalts and dolerites from the Bathani area of the northern fringe of the CGGC, eastern India. The basalts consist of plagioclase feldspar, hornblende, opaque minerals (Fe–Ti oxide) and chlorite, and the dolerite consists of plagioclase, hornblende and opaque minerals. Our data indicate that the Bathani mafic rocks have tholeiitic to transitional composition and are overprinted by greenschist facies metamorphic conditions; however, REE and fluid immobile elements preserve their primary geochemical signatures. The $(La/Sm)_N$ ratios (1.38–2.15) and chondrite-normalized REE patterns point to an enriched mid-ocean ridge basalt (E-MORB) mantle source. Geochemical characteristics indicate a mixed signature of MORB and arc tholeiite with enrichment of Ba, Th, Eu and Sr, similar to that of back-arc supra-subduction zone ophiolites. These mafic rocks are the product of MORB-like magma derived from a depleted mantle corresponding to < 2% partial melting of spinel lherzolite, enriched by subduction-induced slab metasomatism and melting. The Bathani mafic rocks are representative of the upper part of a supra-subduction zone columnar ophiolite section, which was emplaced onto the present-day northern margin of the CGGC during suturing of the northern and southern Indian block at *c.* 1.9 Ga during the Nuna amalgamation.

1. Introduction

The Greater Indian Landmass (GIL) is divided into northern and southern crustal provinces. The Archaean Bundelkhand Craton is the nucleus of the northern crustal province, and the southern province is a composite assemblage of the Dharwar, the Bastar and the Singhbhum Archean Cratons (Acharyya, 2003). The Central Indian Tectonic Zone (CITZ) is an ENE–WSW-trending Proterozoic mobile belt that marks the suture zone between the two crustal provinces. The northern region of the CITZ is occupied by the Mahakoshal Mobile Belt (MMB), which is a narrow rift zone bounded by the Moho-reaching Son-Narmada lineaments. The wider southern belt of the CITZ comprises the Sausar Mobile Belt, the Chotanagpur Granite Gneiss Complex (CGGC) and the Shillong Plateau Gneissic Complex (SPGC).

The CGGC of the east Indian shield is a high-grade terrain located in the eastern part of the CITZ, occupying an area of *c.* 80 000 km^2 (Mahadevan, 2002; Acharyya, 2003) (Fig. 1a). The Quaternary sediments of Gangetic alluvium mostly cover the northern margin of the CGGC with exposures of rocks of the Bihar Mica Belt (BMB), Munger Group and Rajgir–Gaya sub-basins. The sediments of the Bengal Basin mark the eastern margin of the CGGC. Mesozoic volcanics of Rajmahal Trap mark the northeastern fringe of the CGGC, and the western margin is dominantly covered by the Gondwana deposits of Permian – Middle Cretaceous age (Mahadevan, 2002). The northwestern margin of the CGGC is in contact with the Vindhyan and Mahakoshal groups of rocks of Proterozoic age. The southern margin is marked by contact with the North Singhbhum Mobile Belt (NSMB) and the E–W-trending crustal-scale shear zone called the South Purulia Shear Zone of Proterozoic age (Fig. 1a). Multiple magmatic and metamorphic episodes and deformations mark the evolution of the CGGC over a geological history from Proterozoic time until *c.* 65 Ma (Mukherjee & Ghose, 1998). Based on radiometric dates for the CGGC, four magmato-metamorphic events at *c.* > 2.5, 1.6–1.5, 1.2–1.0 and 0.9 Ga (e.g. Chatterjee *et al.* 2008, 2010; Maji *et al.* 2008; Singh & Krishna, 2009; Chatterjee & Ghose 2011; Karmakar *et al.* 2011; PK Mukhopadhyay *et al.*, unpub. report, 2011; Sanyal & Sengupta, 2012; Mukherjee *et al.* 2018; Dey *et al.* 2019) are recognized in the CGGC.

CAMBRIDGE UNIVERSITY PRESS

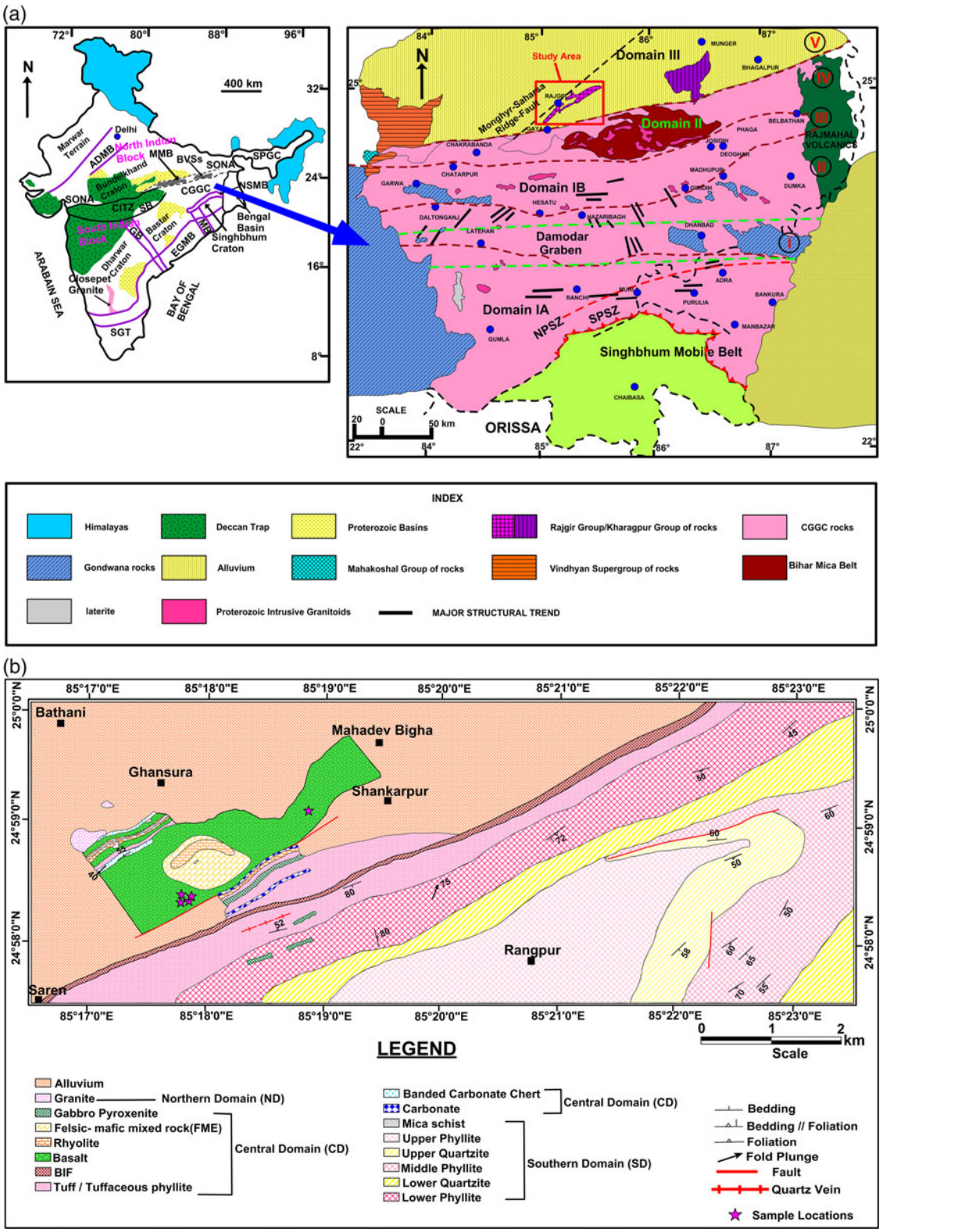

Fig. 1. (Colour online) (a) Left: tectonic map of India showing the location of the Central Indian Tectonic Zone (CITZ) along with other Proterozoic mobile belts of India, including the Eastern Ghats Mobile Belt (EGMB) and the Aravalli Delhi Mobile Belt (ADMB). The CITZ comprises the central CITZ, the Chotanagpur Granite Gneiss Complex (CGGC) and the easternmost Shillong Plateau Gneissic Complex (SPGC). The Bathani Volcano Sedimentary Sequence (BVSS) lies within the ENE–WSW-trending Son-Narmada (SONA) lineaments shown in dashed lines. Four Archaean cratonic nuclei of India, namely Singhbhum, Bastar, Bundelkhand and Dharwar, are also shown (modified after Pradhan *et al*. 2009). GB – Godavari Basin; MB – Mahanadi Basin; MMB – Mahakoshal Mobile Belt; SB – Satpura Basin; NSMB – North Singhbhum Mobile Belt; SGT – Southern Granulite Terrain. Right: CGGC (map modified after Sanyal & Sengupta, 2012). The map represents five subdivisions of CGGC, namely (I) Ranchi–Purulia; (II) Hazaribagh–Dumka; (III) Giridih–Deoghar; (IV) Bihar Mica Belt; and (V) Rajgir–Kharagpur subdivisions as proposed by Mahadevan (2002) delineated by brown lines. Also shown in the map are current subdivisions of CGGC proposed by Mukherjee *et al.* (2019) marked as Domain I (IA and IB), Domain II and Domain III. The red square box shows the study area. NPSZ – North Purulia Shear Zone; SPSZ – South Purulia Shear Zone. (b) Geological map of the area near Bathani village of the Bathani Volcano sedimentary sequence after M Ahmad & AQ Paul, unpub. report (2013). Sample locations are marked in stars.

https://doi.org/10.1017/S0016756821000078 Published online by Cambridge University Press

Mahadevan (2002) classified the CGGC into five E–W divisions based on the Damodar and the Koel river Gondwana basins as reference frames. Mukherjee *et al.* (2019) suggested three roughly E–W-trending domains for the CGGC by integrating the available geochronological, petrological and geochemical data (Fig. 1a); from south to north these are Domain I (IA and IB), Domain II and Domain III. Domain IA includes rocks exposed in the southernmost part of the CGGC and is bounded by the Gondwana Boundary Fault (GBF) to the north and the South Purulia Shear Zone (SPSZ) in the south and comprises variably deformed migmatitic felsic orthogneisses with xenoliths of dismembered rafts of mafic granulite and calc-silicate gneisses. This domain is intruded by massif-type anorthositic rocks. On the other hand, Domain IB is sandwiched between the GBF to the south and Domain II in the north. Domain IB comprises felsic gneiss of granulite grade. Domain II comprises the BMB, and is sandwiched between Domain III in the north and Domain IB in the south. Domain III, at the northern fringe of the CGGC, lies to the north of the BMB. The area exposes an ensemble of migmatitic quartzofeldspathic gneisses and supracrustals. Supracrustals are dominated by quartzite and phyllite in association with mafic–ultramafic and felsic intrusives.

Several tectonic models have been suggested to explain the origin and evolution of the CGGC. (1) Rekha *et al.* (2011) presented a tectonothermal model involving two stages of accretion at *c.* 1560 Ma and 1000 Ma for the evolution of the composite NSMB and CGGC. (2) Sarkar & Saha (1977), Sarkar (1982) and Mahato *et al.* (2008) advocate N-wards subduction of an ancient oceanic crust attached to the Singhbhum Craton beneath the CGGC microcontinent. Continued subduction resulted in collision and annexation of the Singhbhum Craton with the CGGC. (3) Acharyya (2003) proposed S-wards subduction of the northern crustal block beneath the southern crustal block with a continental collision at *c.* 1600–1500 Ma. (4) Mukhopadhyay (1990) and Gupta & Basu (2000) proposed plume-driven rifting between the Singhbhum Craton and the CGGC that led to the formation of an ensialic basin. The present-day NSMB is believed to represent the rift basin. The development of the rift basin was followed by mafic magmatism and crustal shortening. The existence of such varied propositions entails a complex origin and evolution of the CGGC.

The positioning of the CGGC, an eastern continuity of the CITZ, is significant for understanding the supercontinent cycle prevalent during the geological past. Many authors have suggested that the CGGC and Eastern Ghats Mobile Belt (EGMB) were juxtaposed against the East Antarctic Precambrian basement during the existence of the Rodinia supercontinent during Proterozoic time (Dasgupta & Sengupta, 2003; Chatterjee *et al.* 2010). Saikia *et al.* (2017) have also related the granitic magmatism of the Bathani area to the Nuna Supercontinent assembly (2000–1700 Ma). Rocks exposed in various units of the CGGC may therefore provide exciting clues of the magmatism, metamorphism and deformation that accompanied the supercontinent amalgamation and break-up (Mukherjee *et al.* 2019).

Ahmad & Wanjari (2009) reported a NE–SW-trending volcano-sedimentary sequence comprising banded iron formation (BIF), garnet-mica schist, chert bands and mafic–intermediate volcanics from in and around Bathani village in the Gaya district of Bihar from the northern fringe of the CGGC, referred to here as the Bathani Volcano Sedimentary Sequence (BVSS) that falls within the strike continuity of the Mahakoshal Belt. According to the recent classification of the CGGC by Mukherjee *et al.* (2019), the BVSS is a part of Domain III (see Fig. 1a), former Rajgir metasediments and associated granitoids. This discovery is the first preserved magmatic sequence from this highly metamorphosed and deformed northern margin of the CGGC. Ahmad & Wanjari (2009) described the stratigraphy and depositional environment of the BVSS (probably an ophiolitic section) and identified pillow lava basalts and dolerite dykes in the volcano-sedimentary sequence units. However, detailed geochemical characterization and petrographic descriptions of the pillow lava basalts and dolerite dykes from the BVSS of the CGGC have remained undetermined.

We present new geochemical data of the mafic pillow lava and associated dolerite dykes of Bathani area at the northern fringe of the CGGC, and compare the geochemical fingerprints with known and well-studied ophiolite tectonic settings in supra-subduction zones and mid-oceanic ridges to constrain the evolutionary history of mafic rocks of BVSS, in relation to the CGGC. Our findings are significant as the geochemical trends of the studied rocks are highly resonant with the Proterozoic supra-subduction zone ophiolitic lavas, and may have significance for the assembly of the Nuna Supercontinent.

2. Geological background and field relations

The Bathani volcanic sequence is a volcano-sedimentary suite exposed at the northern edges of the CGGC in eastern India with a NE–SW trend (Ahmad & Wanjari, 2009; M Ahmad & AQ Paul, unpub. report, 2013). The aerial extent of all rock variants of the volcano-sedimentary sequence was documented for a strike length of 6 km and width of 5 km. However, extensive geological mapping of BVSS on various scales has revealed a maximum strike extension of 65–70 km from Rajgir in the NE to Jaganathpur in the SW (M Ahmad & AQ Paul, unpub. report, 2013). The type area is located in Bathani (24° 59.5' N, 85° 16′ E) village, Gaya district of Bihar (Fig. 1b). The BVSS can be categorized into three distinct litho-domains from north to south: the northern domain (ND) is represented by intrusive granitoids with xenoliths of volcanics, pyroxenite-gabbro-anorthosite suites; the central domain (CD) comprises low-grade folded differentiated volcano-sedimentary sequence with mafic intrusions; and the southern domain (SD) includes metasedimentary rocks, quartzite and phyllite. The northern litho-domain (ND) represents granitoid rocks that are intrusive within the central volcano-sedimentary litho-domain (CD) (Fig. 1b).

The ND is well exposed around the Nimchak, Bathani, Ghansura and Gaya township area towards the north of the CD. The terrain consists of granite, aplite veins, granodiorite, diorite, mafic magmatic enclaves and xenoliths of rocks of the CD, including banded carbonate chert and basaltic pyroclasts and rocks of pyroxenite-gabbro-anorthosite suites. The granitoids show an intrusive relation with the rocks of the CD, and occur as granite apophyses and cross-cutting aplite veins.

The SD is a meta-sedimentary litho-domain exposed from Rajgir to Gaya for *c.* 65–70 km strike length lying to the south of the volcano-sedimentary CD. A folded sequence of quartzite-phyllite horizons marks the SD. The quartzite-phyllite horizons display sedimentary structures such as graded bedding, trough cross-bedding, ripple marks and syneresis cracks. Dolerite/gabbro dykes and the pyroxenite-gabbro-anorthosite enclaves show an intrusive relation to the central and southern litho-domain of the BVSS.

https://doi.org/10.1017/S0016756821000078 Published online by Cambridge University Press

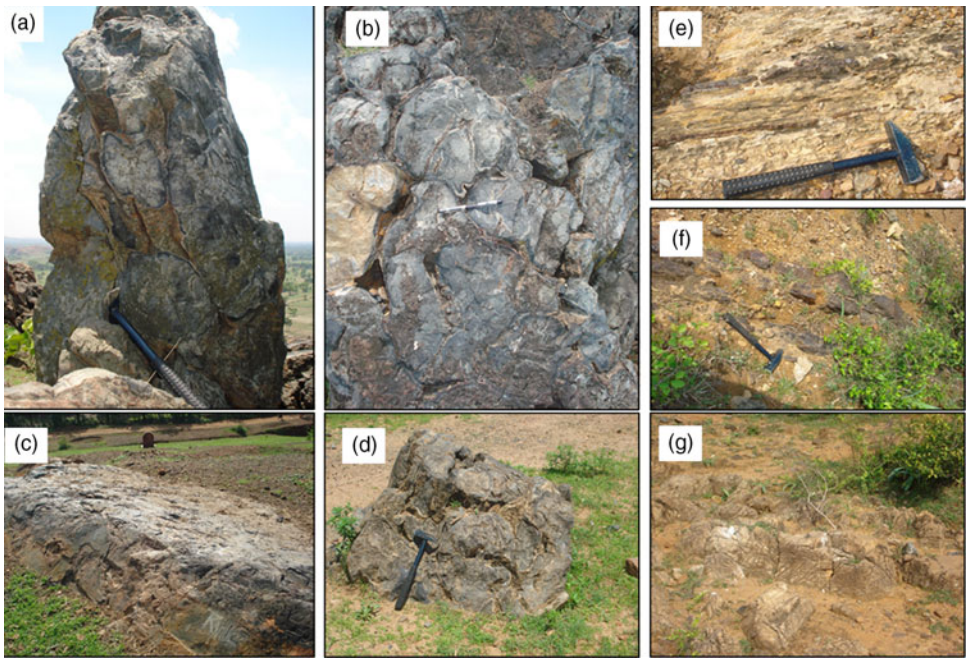

Fig. 2. (Colour online) (a, b) Cross-sectional view of pillows at Churi displaying variation in size and shape, inter-pillow space, rim/rind, vesicles, budding etc. (c) Longitudinal view of pillows at Mahadev Bigha. (d) Irregular shape pillow at Ghansura, loosely packed, inter-pillow space filled with quartz and carbonate. (e) Chert and jasper bands in carbonate (siliceous dolomite) rock. (f) banded iron formations (BIFs) in alternation with tuffaceous layers. Tuff is metamorphosed to tuffaceous phyllite. (g) Typical elephant skin weathering in siliceous dolomite.

The CD consists of tuff, tuffaceous phyllite, banded iron formation (BIF), banded carbonate chert (BCC), carbonate, pillow basalt, massive basalt, andesite, rhyolite and pyroclastics. A garnet-mica-schist band occurs at the contact with granitoids of the ND, and concordant intrusive bodies of pyroxenite-dolerite/gabbro are also observed (Figs 1b, 2). The tuffaceous rocks are spread throughout the area and encompass multiple thin lensoids of BIF, BCC and carbonate (Fig. 2f). Mafic to felsic pyroclastic rocks are exposed near Ghansura village. Basalts are the most widespread volcanic rock from the CD. These basalts are represented by both massive as well as pillowed varieties. The CD extends sporadically for a strike length of 45–50 km from Mahadev Bigha locality in the NE up to Churi and Jaganathpur locality in the SW (Fig. 1b; online Supplementary Fig. S1, available at http://journals.cambridge.org/geo).

No robust chronostratigraphic relations amongst the litho-domains of BVSS is yet established due to a lack of age data from the exposed rock types. However, field relations show that the BVSS unconformably overlies the CGGC. The lowermost unit of the BVSS comprises a pyroxenite-gabbro-anorthosite suite of rocks, which is exposed as enclaves within overlying units. This unit is overlain by the pillow and massive lavas, mafic-felsic pyroclasts, felsic volcanics, felsic tuff, BIF, BCC and limestone occurring as a rock assemblage. Dolerite/gabbro dykes are intrusive in this unit. Clastic sediments, phyllite and quartzite tops this rock assemblage as the sedimentary cover, and granites/granitoids cross-cut this entire litho-domain of the BVSS. Generalized stratigraphy of the area with respect to the CGGC is provided in online Supplementary Table S1.

The focus of the current study is the pillow basalts. Well-preserved pillow basalts are found near Mahadev Bigha and Ghansura villages towards the northeastern extension and near Churi and Jaganathpur towards the southwestern extension of the BVSS (Fig. 2a–d; online Supplementary Fig. S2). The pillows in the basalt of the BVSS are of variable shape and dimension. Their size ranges from small pillow of < 20 cm to mega pillow of > 1 m length of the longer axis. The lower horizon of basalts shows diversity in pillows configuration, for example, spherical, elongated, ellipsoidal, bun, mushroom, kidney, irregular shape, etc. However, in upper flows, pillows are either spherical or elliptical in shape. The pillow structures exhibit well-developed chilled margins, rim/rind, vesicles, cracks, V-up and convex-up features. However, radial cracks in pillows are not frequently observed. The pillows are tightly packed with less inter-pillow space (online Supplementary Fig. S2). Pillow breccias are abundant in Jagannathpur.

Both primary and diastrophic structures are well preserved in the volcano-sediments of the area. The sedimentary structures include mainly compositional and colour banding (S_0) in tuff/tuffaceous phyllite, BIF and BCC. The BCC with alternate chert and carbonate bands shows a rib and furrow structure. The primary magmatic structures in volcanic rocks include primary compositional/colour banding, flow banding, pillows, pyroclasts and vesicular structures. The folded volcano-sedimentary sequence experienced at least three phases of deformation: D_1, D_2 and later D_3. Both mappable and non-mappable closures corresponding to these deformational events have been recognized from the swerving of foliation, attitude of the beds and presence of folded outcrops. The presence of three sets of foliations, the refolding of bedding-parallel foliation and the presence of doubly plunging folds and rootless isoclinal folds are noteworthy features (online Supplementary Figs S3, S4). The area has experienced brittle and brittle-ductile deformation, as indicated by tension gashes showing en échlon sigmoidal shear sense. The normal and thrust faults have been identified in various parts of the volcano-sedimentary sequence. Faults are observed in the form of brecciation, fault gauge, slickensides, silicification, pseudo-tachylite and en échlon pattern of tension gashes at various locations (online Supplementary Fig. S5).

3. Samples and analytical methods

3.a. Outcrops and samples

Mafic rock samples were collected from the Churi, Jagannathpur, Gulani and Bathani villages, Gaya district of Bihar. Ten rock

https://doi.org/10.1017/S0016756821000078 Published online by Cambridge University Press

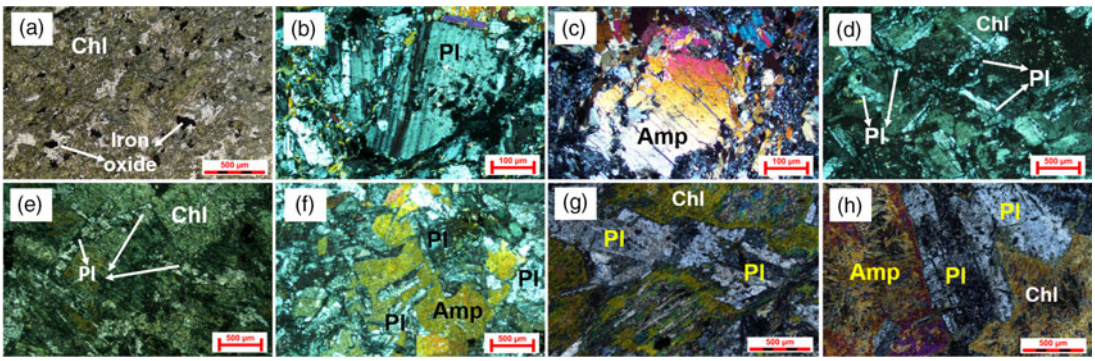

Fig. 3. (Colour online) Photomicrographs. (a) Metamorphosed pillow basalt showing spherulitic texture and greenschist facies mineralogy. (b) Metabasalt showing porphyritic texture. Phenocryst is of saussuritized plagioclase embedded in the fine-grained groundmass of amphibole, chlorite and opaque minerals (c) Metabasalt showing phenocryst of pyroxene, which has altered to amphibole, embedded in a groundmass of altered plagioclase and chlorite. (d) Relics of the porphyritic intergranular texture of an altered basalt. Altered plagioclase crystals can be observed with preserved subhedral to euhedral shapes. (e, f) Altered dolerite shows ophitic texture where laths of plagioclases are enclosed within pyroxenes, which are now altered to chlorite and amphibole. (g, h) Metadolerites showing saussuritization of plagioclase and alteration of pyroxene to amphibole and chlorite.

samples from outcrops of pillow basalts and associated dolerite dykes were taken for petrographic and major- and trace-element studies. The co-ordinates of the samples are given in online Supplementary Table S2. The outcrops occur as massive blocks associated with sedimentary units.

3.b. Analytical methods

Ten representative samples were selected and cut into thin-sections for qualitative petrographic analysis at the University of Delhi, India. All 10 petrographically studied samples were broken into small pieces to remove any trace of veins. The rock samples were crushed and pulverized using agate carbide ring grinder. The major oxides and selected trace-elements analysis were carried out using an X-ray fluorescence spectrometer (XRF) (Bruker S8 Tiger Sequential X-ray spectrometer with Rh excitation source) following the procedure described by Saini *et al.* (1998, 2000). Rare earth elements (REE) were analysed using inductively coupled plasma mass spectrometry at the Wadia Institute of Himalaya Geology, Dehradun, India.

The operating conditions were: no filter, vacuum path and 20–40 kV for the major oxides; and no filter, vacuum path and 55–60 kV for trace elements. The overall accuracy in relative standard deviation (RSD) percentage is 4.5% for major and minor oxides, and 12% for the trace elements. The average precision is better than 2.0% (Purohit *et al.* 2006; Saini *et al.* 2007). Sample solutions were introduced for REE analysis into the argon plasma using a peristaltic pump and a cross-flow nebulizer. The procedures adopted for sample digestion and the preparation of solutions are described in Balaram *et al.* (1990). Samples from the United States Geological Survey (USGS) (Sample BHVO-1) and the Japanese Geotechnical Society (JGS) (Sample JBI 1a) were used as rock standards to minimize the matrix effect. The RSD for most of the samples is better than 10%.

4. Results

4.a. Petrography

Mafic rocks can be identified as basalts and dolerites based on petrography. The basalts display a mineral assemblage typical of lower greenschist facies conditions. They are composed of plagioclase feldspar, amphibole, chlorite and minor opaque minerals (Fe–Ti oxide) (Fig. 3a–d). The phenocrysts are mainly euhedral and subhedral pseudomorphs of amphibole (Fig. 3c) after pyroxene. Plagioclases commonly show replacement by albite and saussurite (Fig. 3a, b) in most of the basalt samples. However, the plagioclases of sample RJ8 show extensive sericitization. Chlorite and amphibole usually replace pyroxene in the samples (Fig. 3d). The groundmass of the basalt displays intergranular or intersertal textures. It is composed of long columnar or acicular plagioclase, rhomboidal pale-brown amphibole, acicular or fibrous pale-green amphibole. Some of the metabasalts display plagioclase grains preserved within a matrix composed of chlorite and carbonate minerals (Fig. 3d).

Dolerite consists of plagioclase, hornblende and opaque minerals. Dolerites exhibit ophitic to sub-ophitic textures. Ophitic to sub-ophitic textures are usually observed where plagioclase laths are enclosed partially or entirely within pyroxenes, now amphiboles and chlorites (Fig. 3e–g). The plagioclases are saussuritized, and the clinopyroxenes are typically replaced by secondary amphibole or chlorite (Fig. 3g, h).

4.b. Geochemistry

Major- and trace-element data and selected inter-element ratios of 10 samples of mafic rocks of BVSS are presented in Table 1, and their geochemical signatures are described below.

The major-element composition is consistent with the compositional range of basalts and dolerites in which moderate variations are observed. In basalts the variations are: SiO_2, 43.67–49.83 wt%; Al_2O_3, 8.9–18.6 wt%; TiO_2, 1.6–2.57 wt%; Fe_2O_3, 8.96–18.79 wt%; MgO, 5.4–8.25 wt%; CaO, 10.39–15.39 wt%; K_2O, 0.17–0.79 wt% (except for one sample RJ8 with K_2O content of 4.3 wt%); and Na_2O, 0.79–2.8 wt%. The variations in dolerites are: SiO_2, 45.08–46.72 wt%; Al_2O_3, 14.03–14.07 wt%; TiO_2, 0.72–0.79 wt%; Fe_2O_3, 12.01–13.38 wt%; MgO, 10.07–11.15 wt%; CaO, 9.25–10.55 wt%; K_2O, 0.33–0.5 wt%; and Na_2O, 2.07–2.54 wt%.

The Mg no. for basalt varies from 37.3 to 64.4 and for dolerites is *c.* 62. The Mg no. is calculated based on the formula $100 \times (MgO/40.32)/[(MgO/40.32) + (FeO/71.85)]$, where FeO is calculated from Fe_2O_3 by using a conversion factor of 0.8998. The studied rocks display low loss on ignition (LOI) values (0.3–3.75 wt%). The fluid mobile large-ion lithophile elements (LILE) concentrations are: Rb, 3–99 ppm; Sr, 124–376 ppm; and Ba,

https://doi.org/10.1017/S0016756821000078 Published online by Cambridge University Press

Table 1. Major oxides, trace and rare earth elements composition of the pillow lava basalts and dolerites from the Bathani volcano-sedimentary sequence of CGGC. BDL – below detection limit.

Rock type	Basalt								Dolerite	
Sample	RJ1	RJ8	RJ16C	RJ37A	RJ37B	RJ38	RJ35	RJ34	RJ15	RJ19
Major oxide (wt%)										
SiO_2	49.43	42.81	47.63	46.63	47.42	47.90	43.67	48.78	46.72	45.08
TiO_2	2.51	1.60	2.49	1.47	2.20	1.71	2.05	2.57	0.79	0.72
Al_2O_3	10.09	18.60	11.98	12.74	11.22	12.19	8.90	10.62	14.03	14.07
Fe_2O_3	15.62	8.96	16.75	14.93	18.79	17.25	18.36	18.05	12.01	13.38
MnO	0.20	0.16	0.20	0.22	0.27	0.29	0.26	0.25	0.18	0.21
MgO	5.40	8.25	5.62	7.54	5.93	5.87	6.88	5.44	10.07	11.15
CaO	11.17	10.41	10.52	11.82	10.39	10.53	15.39	10.52	9.25	10.55
Na_2O	2.80	1.52	2.14	1.99	1.66	1.78	0.79	1.50	2.54	2.07
K_2O	0.60	4.33	0.79	0.17	0.39	0.26	0.51	0.29	0.50	0.33
P_2O_5	0.28	0.17	0.25	0.14	0.23	0.20	0.20	0.22	0.06	0.05
LOI	0.63	3.75	1.06	0.93	0.56	0.60	1.16	0.30	2.12	2.42
Total	98.73	100.56	99.43	98.58	99.06	98.58	98.17	98.54	98.27	100.03
Trace elements (ppm)										
Ba	167	151	223	122	145	73	195	131	238	127
Cr	267	358	306	277	194	156	205	391	489	484
V	416	397	430	321	466	381	386	441	196	213
Sc	43	62	46	53	51	47	43	48	39	39
Co	51	118	61	68	61	65	46	57	60	69
Ni	49	429	89	104	54	72	43	51	229	282
Cu	41	182	113	149	133	57	195	166	158	96
Zn	115	84	138	103	178	128	172	144	92	110
Ga	20.36	22.75	20.58	19.68	20.31	20.31	20.99	23.79	15.81	16.35
Pb	7.8	569.2	4.7	5.7	3.3	24.2	1.6	2.4	45.9	93.4
Rb	17	99	32	3	11	5	11	4	15	6
Sr	234	145	226	215	151	284	124	185	376	240
Y	47	35	48	29	47	36	43	46	18	16
Zr	196	106	173	83	135	113	151	182	33	23
U	BDL	BDL	BDL	BDL	BDL	BDL	BDL	BDL	BDL	BDL
Th	1.33	BDL	2.25	2.13	1.42	1.41	2.9	2.25	0.29	0.55
REE (ppm)										
La	19.40	5.20	16.20	7.40	11.70	9.10	11.60	12.10	5.00	3.30
Ce	45.50	13.20	39.30	18.00	28.50	22.10	29.40	30.50	10.10	7.10
Pr	6.40	2.00	5.50	2.70	4.20	3.40	4.40	4.50	1.30	1.00
Nd	28.10	9.20	24.20	11.90	18.30	15.40	19.90	20.50	5.60	4.30
Sm	7.08	2.57	6.25	3.26	5.00	4.27	5.32	5.50	1.50	1.24
Eu	2.19	0.92	2.14	1.20	1.63	1.42	1.73	1.75	0.65	0.58
Gd	8.27	2.84	7.06	4.02	6.03	5.00	6.13	6.33	1.84	1.59
Tb	1.37	0.50	1.17	0.70	1.04	0.86	1.02	1.09	0.33	0.30
Dy	8.41	3.00	7.03	4.39	6.69	5.31	6.30	6.52	2.06	1.90
Ho	1.78	0.63	1.48	0.95	1.46	1.14	1.30	1.36	0.45	0.42
Er	4.71	1.66	3.89	2.53	3.96	3.00	3.37	3.58	1.22	1.13
Tm	0.71	0.24	0.58	0.39	0.61	0.46	0.50	0.54	0.19	0.17

(*Continued*)

https://doi.org/10.1017/S0016756821000078 Published online by Cambridge University Press

Table 1. (*Continued*)

Rock type	Basalt								Dolerite	
Sample	RJ1	RJ8	RJ16C	RJ37A	RJ37B	RJ38	RJ35	RJ34	RJ15	RJ19
Yb	4.53	1.56	3.75	2.54	4.02	2.95	3.14	3.48	1.28	1.16
Lu	0.65	0.23	0.56	0.38	0.61	0.45	0.46	0.52	0.20	0.17
Mg no.	40.65	64.59	39.93	37.38	42.60	50.01	38.47	40.27	62.42	62.27
Sr/Rb	13.76	1.46	7.06	71.67	13.73	56.80	11.27	46.25	25.07	40.00
K/Ba	29.83	238.04	29.41	11.57	22.33	29.57	21.71	18.38	17.44	21.57
K/Rb	292.99	363.08	204.94	470.41	294.32	431.67	384.88	601.84	276.71	456.57
Zr/Ti	0.01	0.01	0.01	0.01	0.01	0.01	0.01	0.01	0.01	0.01
Nb/Y	0.40	0.22	0.38	0.29	0.29	0.24	0.24	0.27	0.48	0.38
Nb/Yb	4.17	5.00	4.80	3.27	3.38	2.98	3.25	3.56	6.80	5.17
Zr/Y	4.17	3.03	3.60	2.86	2.87	3.14	3.51	3.96	1.83	1.44
Ti/V	36.17	24.16	34.72	27.45	28.30	26.91	31.84	34.94	24.16	20.26
Nb/Zr	0.10	0.07	0.10	0.10	0.10	0.08	0.07	0.07	0.26	0.26
Nb/La	0.97	1.50	1.11	1.12	1.16	0.97	0.88	1.02	1.74	1.82
$(La/Sm)_N$	1.77	1.31	1.67	1.42	1.41	1.47	1.51	1.38	2.15	1.72
Sr/Sr*	0.76	1.09	0.84	1.53	0.67	1.50	0.58	0.81	5.87	4.68
Ti/Ti*	0.82	1.44	0.94	0.99	0.98	0.91	0.9	1.07	1.14	1.2
Sr/Y	4.98	4.14	4.71	7.41	3.21	7.89	2.88	4.02	20.89	15
Eu/Eu*	0.87	1.04	0.98	1.01	0.91	0.94	0.93	0.91	1.2	1.26
Nb	19	8	18	8	14	9	10	12	9	6

73–238 ppm. To find the mineralogically altered primary rock composition of the rock, we adopted a rock classification diagram based on immobile element ratios. The immobile element ratio diagrams remove the elemental mass change effect produced by the hydrothermal alteration. The high-field-strength element (HFSE) ratio of altered rock is similar to the HFSE ratio of parent rock (Finlow-Bates & Stumpfl 1981; MacLean & Barrett, 1993). The HFSE classification diagram is therefore preferred for altered rocks. All the studied samples plot in the field of basalt of Zr/Ti versus Nb/Y discrimination diagram (online Supplementary Fig. S6) after Pearce (1996). Variation diagrams of selected major elements (SiO_2 and K_2O) and fluid mobile elements (Ba and Sr) do not display systematic correlations with Zr contents (Fig. 4a–d). Zr was chosen to be plotted against other elements in bivariate plots as it is considered to be one of the least mobile elements; it is therefore used as an alteration independent index of geochemical variations in modern volcanic rocks (Winchester & Floyd, 1977; Pearce & Peate, 1995; Polat *et al.* 2002). The fluid immobile elements display moderate variations in Ti (4316–15 046 ppm), V (196–441 ppm), Th (0–2.25 ppm), Yb (0.88–4.53 ppm), Nb (3.8–18.9 ppm), Y (16–47 ppm), La (3.3–19.4 ppm) and Sm (1.5–7.08 ppm). Selected fluid immobile elements (TiO_2, Sm, Nb and Gd) display systematic correlations with Zr contents (Fig. 4e–h), and ratios of Zr/Ti = 0.05–0.01, Nb/Y = 0.22–0.48, Ti/V = 20.26–36.17 and $(La/Sm)_N$ = 1.31–2.15 are consistent with the transitional nature of basalts between tholeiitic and calc-alkaline. The transitional nature of magma is further confirmed by discrimination diagram based on the immobile element of Y versus Zr (online Supplementary Fig. S7).

On the chondrite-normalized REE diagram, the studied mafic rocks display slight enrichment of LREEs ($(La/Yb)_N$ = 1.71–3.88; $(Gd/Yb)_N$ = 1.18–1.74) relative to HREEs (Fig. 5a). Studied samples display variable Eu/Eu* values (0.87–1.26), suggesting fractionation of plagioclase. The sum of REEs ranges from 43.75 to 119.11 for basalts and from 24.36 to 31.72 in the dolerites. These values, along with the subparallel nature of the trend in REEs, indicate the cogenetic nature of these rocks. On normal mid-ocean ridge basalat (N-MORB) normalized trace-element diagram (Fig. 5b), the mafic rocks display elevated concentrations of slab-derived components such as K, Rb, Sr, Ba, Th and Pb relative to the conservative mantle-wedge-derived components such as Ti, Zr, Nb, Sm, Eu, Dy, Yb and Lu.

5. Discussion

5.a. Post-magmatic alteration

Petrographic observations show that the mafic rocks of the Bathani area have experienced greenschist facies metamorphism. The amphiboles and chlorites are interpreted as metamorphic minerals that have entirely replaced magmatic counterparts, most likely pyroxene. Plagioclase occurs as laths, reflecting typical magmatic textures in the mafic pillows. The replacement of original pyroxene crystals by amphiboles without any change in original igneous textures suggests isochemical changes and volume to volume replacement (Redman & Keays, 1985). The observed modification in the magmatic textures and primary minerals of the BVSS basalts is

https://doi.org/10.1017/S0016756821000078 Published online by Cambridge University Press

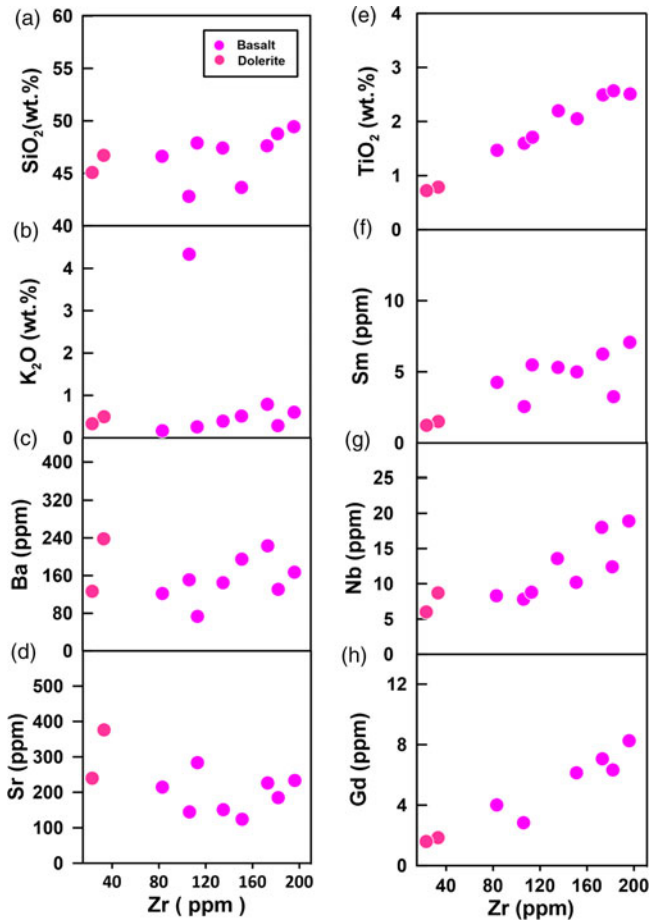

Fig. 4. (Colour online) Bivariate diagrams. (a–d) Zr versus selected major elements such as SiO_2 and K_2O and fluid mobile elements such as Ba and Sr. (e–h) Zr versus selected fluid immobile elements such as TiO_2, Sm, Nb and Gd. Major elements and fluid mobile elements show non-correlating behaviour. In contrast, the fluid immobile elements show a correlating trend.

possibly connected with the metamorphic event reported in the CGGC spaning 1.6–1.5 Ga during the Mesoproterozoic Era (Maji *et al.* 2008; Chatterjee *et al.* 2010; Karmakar *et al.* 2011; Rekha *et al.* 2011). Further, the mafic samples of our study display variations in major elements and LILEs. No clear correlation can be ascertained for the Zr behaviour against major elements and LILE of these samples (see Fig. 4). The LOI values (0.3–3.7 wt%) seem to have been affected by the post-magmatic alteration process. Most likely, the LOIs are increased by the presence of amphibole and chlorites in the samples. However, the absence of Ce anomaly and the lack of any tight correlation of major oxides, HFSE and LILE with the LOI values suggest that these elements were not significantly modified by the metamorphism or any other secondary alteration process.

Several studies have established that major elements, LILE (K, Rb, Na, Sr, Ba, U and Pb) and LREE are susceptible to redistribution during metamorphism as a result of their high mobility. In contrast, Nb, Ti, Zr and Y and HREE are relatively immobile during alteration processes (Pearce & Norry, 1979; Valsami & Cann, 1992). The petrogenetic inferences of the studied rocks are therefore based on the assessment of geochemical signatures of the fluid immobile elements.

5.b. Magmatic evolution

Mafic magma experiences open-system processes such as crustal contamination and fractional crystallization; these processes may change the chemical compositions of the primary mafic magma during its passage through the continental crust to variable extents. The potential influence of such processes should therefore be assessed before constraining the nature of parental magma for the mafic rocks of the BVSS.

Melt derived from the mantle is susceptible to crustal contamination through ascent or temporary residence in crustal magma chambers (Watson, 1982; Mohr, 1987; Pe-piper *et al.* 2003). The continental crust is enriched in LILEs and LREEs and depleted in HFSEs. The assessment of ratios, namely Ti/Y, Ba/Nb, La/Yb, La/Sm, Ba/Zr, Zr/Y, $(Nb/Yb)_{PM}$, $(Th/Yb)_{PM}$ and Nb/Y, is therefore routinely used in evaluating the crustal contamination (Rollinson, 1993). Trace-element ratio diagrams for Bathani mafic rocks are shown in Figure 6a–c. Plots show that studied basalts follow the mantle array except for the dolerites. Samples plotting away from the mantle array are likely affected by lower continental crustal (LCC) contamination. The elemental ratios such as Zr/Nb (3.66–15.16) and Ba/Nb (8.11–26.44) in the studied basalts are lower than those for continental crust (Zr/Nb = 16.2; Ba/Nb = 54; Hofmann *et al.* 1986), which indicates that they probably lack continental lithospheric sources. The studied mafic rocks also have La/Nb ratios (0.55–1.13) similar to the asthenospheric mantle (La/Nb < 1) and lower than the lithospheric mantle (La/Nb > 1) (Fitton *et al.* 1988; Thompson & Morrison, 1998), suggesting an origin from the asthenospheric mantle. The origin of the rocks from asthenospheric mantle source is further corroborated by the ratio diagram of (La/Yb) versus (Nb/La) of Smith *et al.* (1999) (Fig. 7a). Moreover, in crustal contamination, the bulk composition of rocks shifts towards andesitic composition with higher SiO_2 and low MgO. On the contrary, the integration of the subduction component into the mantle would not ensue any such change in the bulk composition (Rudnick & Gao, 2003; Hollings *et al.* 2012; Ernst, 2014). Our samples display a lower abundance of SiO_2 (< 49.43 wt%), a higher abundance of MgO (5.85–11.15 wt%), Ni (43–429 ppm) and Cr (156–628 ppm), and a lower abundance of Th (< 2.2 ppm). These signatures of available bulk rock data of our samples rule out significant crustal contamination as the dominant process. Rather, the trace-element characteristic of Bathani mafic rocks can be attributed to an enriched mantle source rather than crustal contamination.

The enrichment of LILE and depletion of HFSE in the studied samples can be a characteristic of the mantle source, which may be attributed to subduction-related mantle metasomatism. Generally, enrichment/metasomatism can take place in two ways: either by hydrous melts or by slab-derived fluids in subduction systems (Saunders *et al.* 1991; Pearce & Parkinson, 1993; Pearce & Peate, 1995; Gribble *et al.* 1996; Hawkesworth *et al.* 1997; MacDonald *et al.* 2000; Elburg *et al.* 2002). Several studies on mantle metasomatism have revealed that proxies such as REE, Th, and Ba behave differently in slab-derived fluid and slab-derived melts (e.g. Kogiso *et al.* 1997; Woodhead *et al.* 2001; Spandler & Pirard, 2013). The use of these proxies can therefore easily identify the role of fluids and melts derived from subducted oceanic crust and sediments (Guo *et al.* 2015). As illustrated in the plot of Th/Sm versus Th/Ce, the Bathani mafic rocks show a sediment input trend (Fig. 7b) probably indicative of sediment-related melt enrichment. In ratio plots of Rb/Y versus Nb/Y (Fig. 7c) and Nb/Zr versus

https://doi.org/10.1017/S0016756821000078 Published online by Cambridge University Press

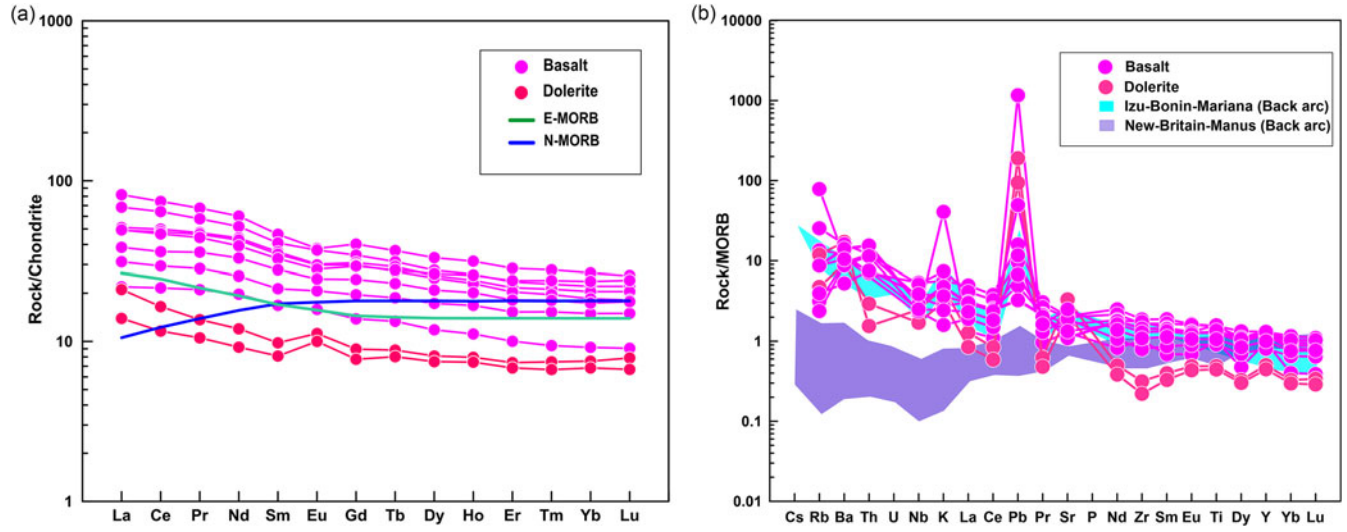

Fig. 5. (Colour online) (a) Sample/chondrite-normalized rare earth element trends of Bathani mafics; normalizing data from Sun & McDonough (1989). (b) Sample/MORB normalized trace-element spidergrams; normalizing data from Hofmann (1988). For comparison purposes, trace-element data in blue and purple patterns plotted from the Izu–Bonin–Mariana and New Britain–Manus back-arc basins. Data source: Metcalf & Shervais (2008).

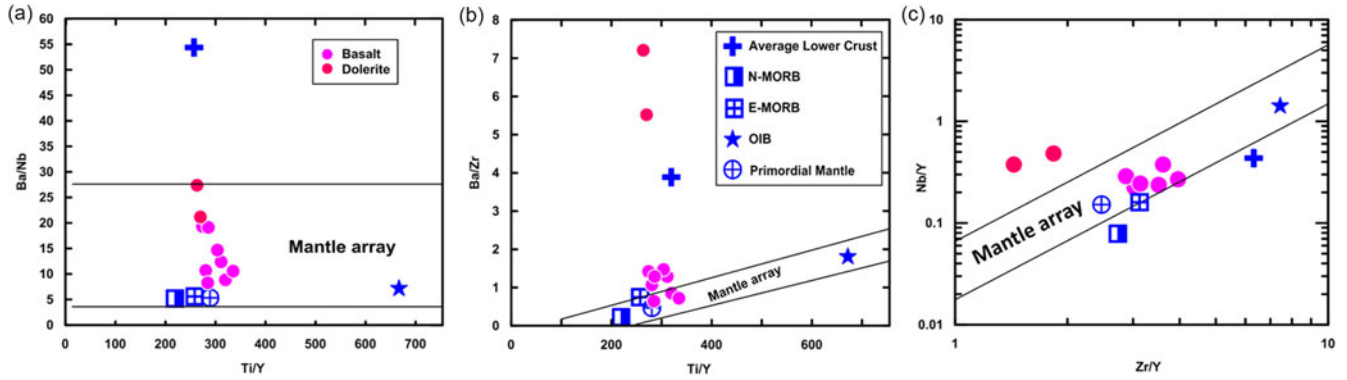

Fig. 6. (Colour online) (a) Ti/Y versus Ba/Zr; (b) Ti/Y versus Ba/Nb; and (c) Nb/Y versus Zr/Y variation diagrams of the mafic rocks of the BVSS. Average lower crust (+; Weaver and Tarney, 1984), N-MORB (half-filled square; Humphris *et al.* 1985), E-MORB (open square; Humphris *et al.* 1985), OIB (star; Sun, 1980), primordial mantle (circle; after McDonough & Sun, 1995). The value of average continental crust (+) is from Rudnick & Fountain (1995) and Rudnick & Gao (2003).

Th/Zr (Fig. 7d), all the studied samples indicate that melt-related enrichment by sediment metasomatism has played a dominant role in the evolution of the mafic magma. It can be inferred that the mafic rocks of the Bathani area have been derived from a depleted mantle source that was modified mainly by the subduction-related sediments with subordinate influence from the fluid-derived melt.

It is widely accepted that primary mantle-derived melts generally have Mg no. > 70, Cr > 1000 ppm and Ni > 400 ppm (Yan *et al.* 2018). The mafic rocks of the BVSS have much lower values for Mg no. (37.38–62.42), Cr (156–489 ppm) and Ni (49–282 ppm, except for sample RJ8), indicating the substantial role of fractional crystallization. Low concentrations of MgO, CaO and compatible elements indicate fractionation of clinopyroxene in the studied rocks. The positive correlation between Cr and Ni also favours the fractionation of clinopyroxene in the studied samples (online Supplementary Fig. S8a). In contrast, the positive correlations of Eu/Eu* with Sr/Y and Sr/Sr* and a negative correlation between Eu/Eu* and total REE indicate the role of plagioclase fractionation (online Supplementary Fig. S8b–d). However, for the dolerite samples (RJ15 and RJ19), Eu/Eu* > 1.0, suggesting plagioclase accumulation is responsible for the positive Eu anomalies observed for these samples. Fractionation and/or accumulation of pyroxene and plagioclase in the magma chamber were therefore responsible for forming the BVSS mafics.

5.c. Depth constraints, partial melting and mantle source

In chondrite-normalized REE patterns, magmas generated by partial melting of a garnet-lherzolite mantle source are known to exhibit relatively high fractionation of HREEs due to the presence of residual garnet, whereas magmas generated from partial melting of a spinel lherzolite source display flat REE patterns (e.g. Hirose & Kushiro, 1993). The chondrite-normalized REE plot of Bathani mafic rocks display relatively flat HREE patterns ($(Dy/Yb)_{CN} = 0.89–1.74$), suggesting their formation by partial melting of a mantle source in the spinel stability field. Further, the melting of the plagioclase-bearing mantle would generate quartz tholeiitic basalts (e.g. Hansen *et al.* 2019), which is not the case with Bathani mafic rocks. The primary magma for the

https://doi.org/10.1017/S0016756821000078 Published online by Cambridge University Press

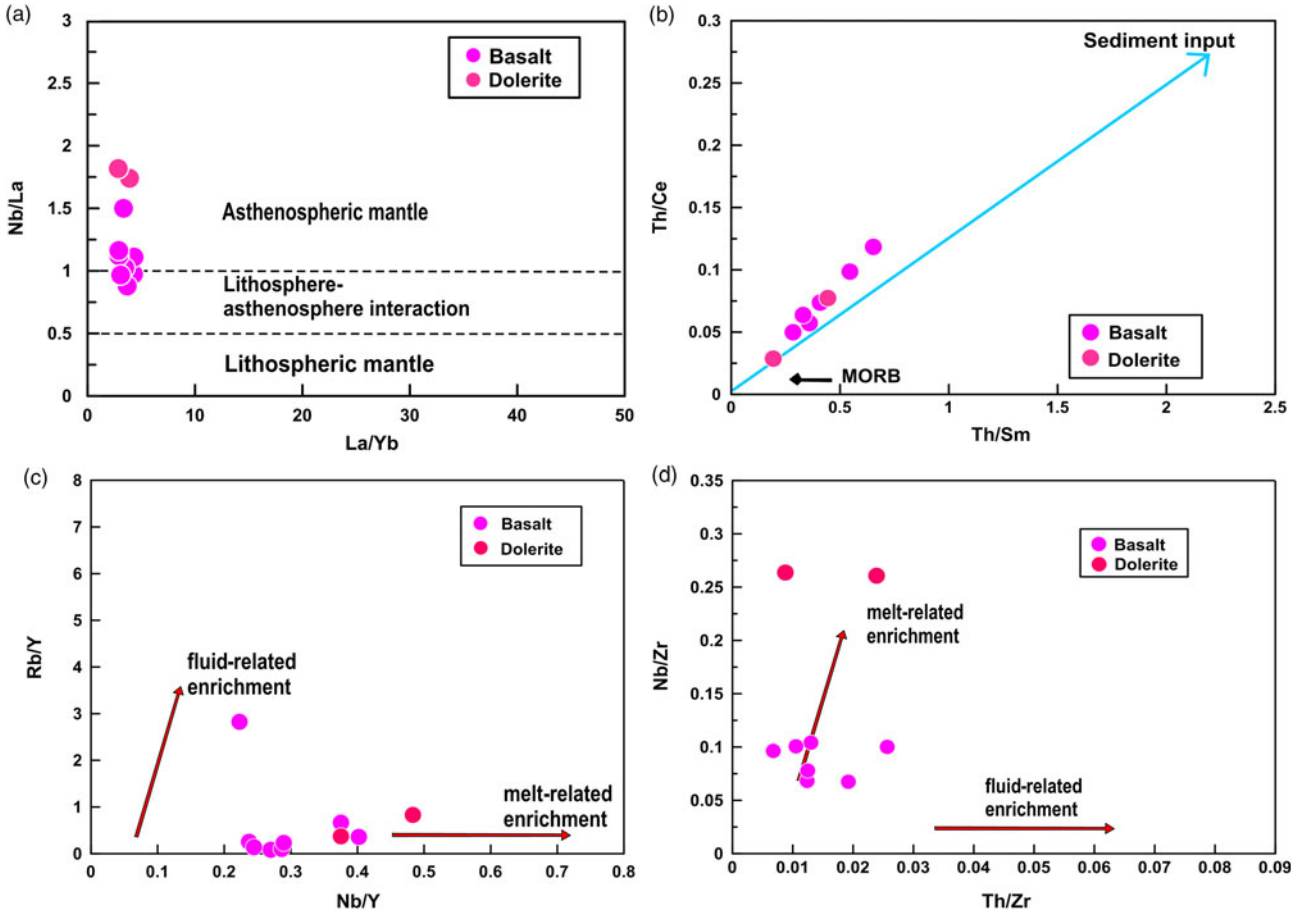

Fig. 7. (Colour online) (a) La/Yb versus Nb/La (Smith *et al.* 1999) plot shows enriched mantle source for Bathani mafics. (b) Th/Sm versus Th/Ce diagrams of the Bathani mafics showing the involvement of subducted sediment in the depleted mantle. (c) Nb/Y versus Rb/Y (d) Nb/Zr versus Th/Zr, indicating melt addition in Bathani mafics.

Bathani mafic therefore probably formed between pressures $P < 2.8$ GPa (Robinson & Wood, 1998) and $P > 0.8$–0.7 GPa (Borghini *et al.* 2010), corresponding to depths of < 85 km and > 30 km (where depth is calculated as $(3.02 \times P$ in kbar$) + 5$; Scarrow & Cox, 1995), respectively.

Three types of melting – batch, fractional and dynamic – models are generally used to estimate the degree of partial melting in the source. During batch (equilibrium) melting, a finite amount of melt is produced that equilibrates with the solid residue. The melt is extracted during fractional melting as soon as it is produced, and very little amount will be in equilibrium with the solid residue. Dynamic melting is based on the principle that melt in excess of source porosity is extracted at the same rate at which it is produced (e.g. Zou & Zindler, 1996). Batch melting model is usually applied for homogenous rocks where the mineral phases appear to be in equilibrium. However, robust quantification of the melting processes that produced Bathani mafic rocks is difficult as mantle source compositions are hard to constrain. Nonetheless, semi-quantitative REE modelling has been widely used to constrain the source for mafic rocks associated with various tectonic settings (Montanini *et al.* 2008; Saccani *et al.* 2013*a*, *b*, 2014; Liu *et al.* 2018).

Here, we use the non-modal batch melting calculations (after Shaw, 1970) to estimate the degree of partial melting (F) of a mantle source that produced the Bathani basaltic rocks. Chondrite-normalized REE patterns of Bathani basalt suggest partial melting of source in the spinel stability field, as discussed in Section 5.b.

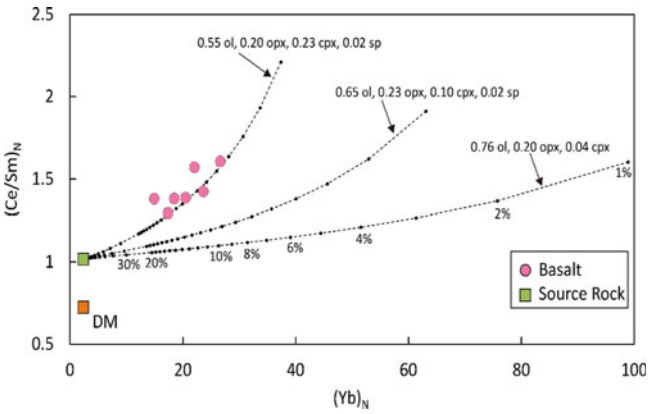

Fig. 8. (Colour online) $(Yb)_N$ versus $(Ce/Sm)_N$ plot for Bathani basalt samples. Dashed black lines are melt curves at variable residual mineral modes, and filled circles represent the percent of partial melt fractions. Source rock is spinel lherzolite (Sample s_S-32; Carlson & Ionov, 2019). Residual mineral mode 0.55 ol, 0.20 opx, 0.23 cpx and 0.02 sp best represent Bathani basalt samples. Partition coefficients from McKenzie & O'Nions (1991). Normalizing chondrite values from Sun & McDonough (1989). Depleted mantle (DM) composition after Salter & Stracke (2004). ol – olivine; opx – orthopyroxene; cpx – clinopyroxene; sp – spinel.

Non-modal batch melting of a depleted mantle source (DM; Salters & Stracke, 2004) produces partial melts with more depleted LREE trends than the Bathani basalt. It can therefore be inferred

https://doi.org/10.1017/S0016756821000078 Published online by Cambridge University Press

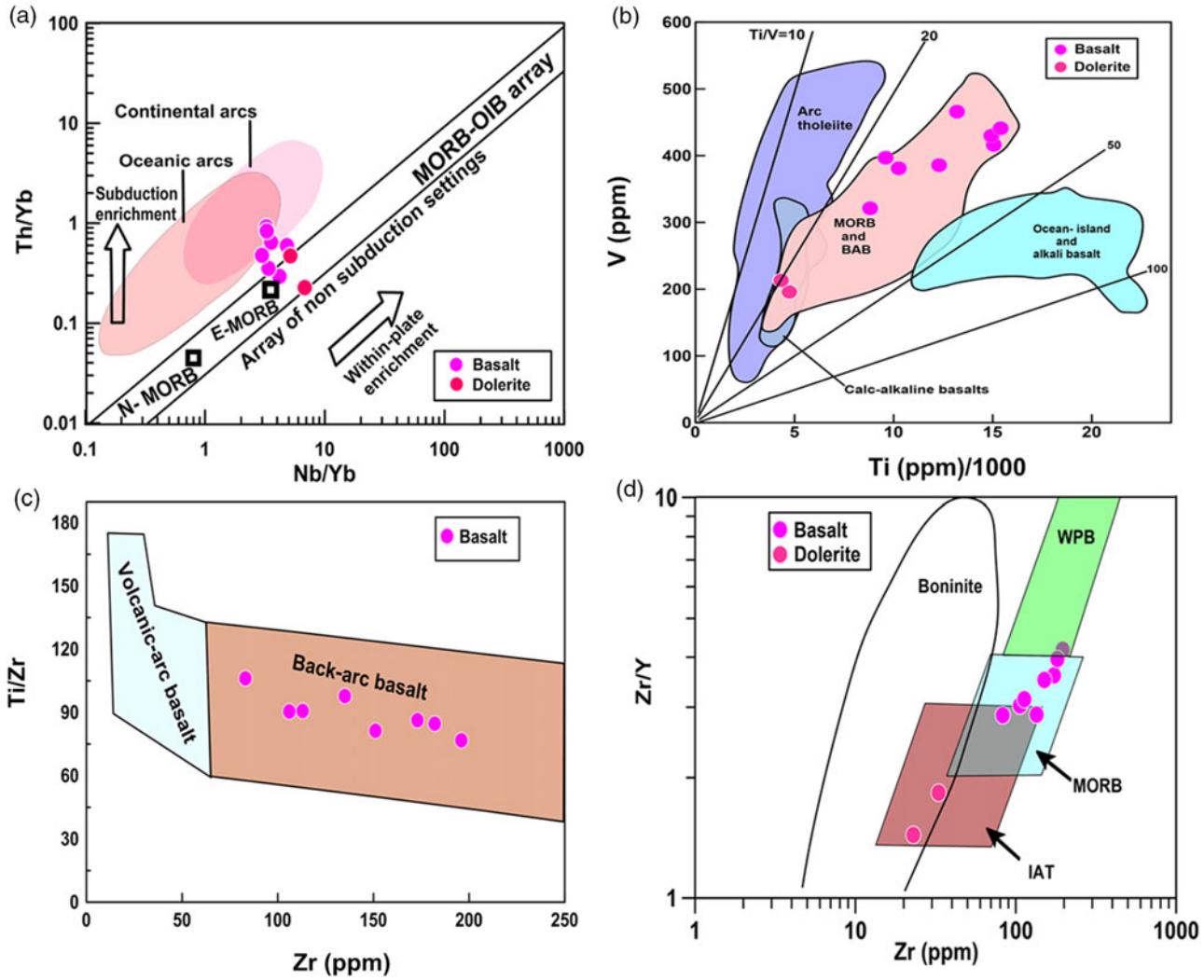

Fig. 9. (Colour online) (a) Nb/Yb versus Th/Yb plot after Pearce (2008) for the studied samples of Bathani mafics showing compositional similarity to E-MORB. (b) Ti versus V plot of the Bathani mafics (Ti/V ratios: island arcs, 10–20; MORB, 20–50; mixed MORB and island arc, 20–30; back-arc basins, 10–50) and boninite field; diagram after Shervais (1982). (c) Discrimination of back-arc basalt affinity of the Bathani mafics rocks on Ti/Zr versus Zr (Woodhead *et al*. 1993). (d) Zr versus Zr/Y tectonic discrimination diagram (after Pearce & Norry, 1979) showing mixed signatures of island arc and MORB for Bathani mafics. IAT – island-arc tholeiite; MORB – mid-oceanic ridge basalt; WPB – within-plate basalt.

that an LREE composition slightly more enriched than DM is the most credible source for the studied samples. After a trial, it was found that slightly LREE enriched spinel lherzolite of Carlson & Ionov (2019; sample s_S-32) produced melts that are near-parallel to the Bathani mafic at variable degrees of partial melting. The inferred mantle source composition is similar to the primitive mantle (Sun & McDonough, 1989).

The possible range of residual mineral modes in the source can be inferred from naturally occurring spinel lherzolites. The effects of source composition and residual mineralogy on partial melting are better constrained in the $(Yb)_N$ versus $(Ce/Sm)_N$ binary plot (e.g. Hansen *et al.* 2019). Figure 8 is a $(Yb)_N$ versus $(Ce/Sm)_N$ binary plot for Bathani basalt samples. Partial melts generated by non-modal batch melting of the inferred source (sample s_S-32; Carlson & Ionov, 2019) at variable mineral modes are also shown. Figure 8 demonstrates that partial melt generated by residual mineral mode olivine 55%, orthopyroxene 20%, clinopyroxene 23% and spinel 2% is best suited to the Bathani basalt samples. Here, the Bathani basalt samples are well constrained within F = 4–12%.

5.d. Tectonic setting and geodynamic implications

The trend of the N-MORB normalized trace elements of the studied mafic rocks has a strong resemblance to the back-arc basalts with enriched MORB (E-MORB) affinity as for those from the Izu–Bonin–Mariana back-arc. A pronounced enrichment in highly incompatible elements such as Cs, Rb and Th are consistent with back-arc basin basalts of subduction environment. The Th/Yb versus Nb/Y discrimination diagram shows the composition of the mafic rocks clustering near E-MORB composition (Fig. 9a) showing similarity to basalt that erupts in general back-arc tectonic settings (Metcalf & Shervais, 2008). Furthermore, the tectonic setting of altered mafic rocks can be robustly constrained by evaluating the fluid immobile elements such as Ti, V, Zr and Y. In Figure 9b, Ti/V ratios for the studied samples range over 20.26–36.17 and fall within the MORB and back-arc basin tectonic settings (Shervais, 1982). The Ti/Zr versus Zr discrimination diagram after Woodhead *et al.* (1993) show the back-arc basin affinity of the Bathani mafics rocks (Fig. 9c). However, Zr/Y versus Zr plots displayed mixed signatures of MORB and arc lavas (Fig. 9d). The observed hybrid mixture between MORB and arc-like elemental

https://doi.org/10.1017/S0016756821000078 Published online by Cambridge University Press

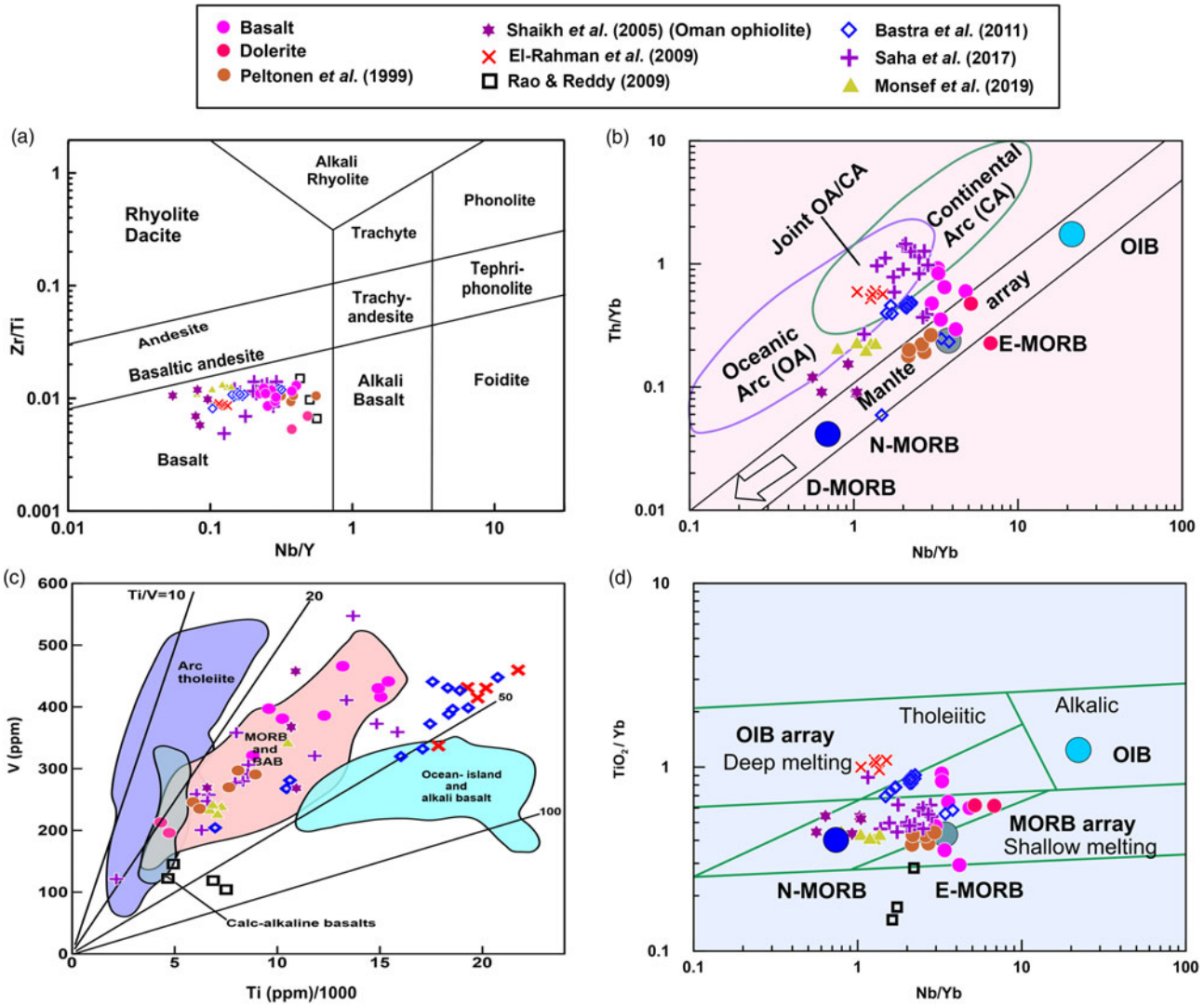

Fig. 10. (Colour online) Various diagrams used for geochemical classification and tectonic discrimination of tectonic settings of ophiolitic crustal units after Pearce (2014) were adopted in this paper to compare our mafic rock data with Proterzoic ophiolitic mafics. (a) Zr/Ti–Nb/Y diagram from Floyd & Winchester (1975). (b) Th/Yb–Nb/Yb and (d) TiO_2/Yb–Nb/Yb diagrams after Pearce (2008). (c) V–Ti/1000 diagrams after Shervais (1982) and modified by Pearce (2014). Data used for comparison are from Indian occurrences of Proterozoic ophiolites: Palaeoproterozoic Kandra Ophiolite Complex, Southern India and Proterozoic ophiolite melange Nellore–Khamman schist belt, SE, India: Saha *et al.* (2017); world occurrences of Proterozoic ophiolites: Rao & Reddy (2009); Neoproterozoic Wadi Ghadir ophiolite, Eastern desert, Egypt: El-Rahman *et al.* (2009); 1.95 Ga Jormua Ophiolite, North Eastern Finland: Peltonen *et al.* (1996); Neoproterozoic Wadi Ghadir Ophiolite, NE Africa, and Cretaceous Ophiolite: Basta *et al.* (2011); Cretaceous ophiolite volcanic suite, Ghayth area Oman: Shaikh *et al.* (2005); Late Cretaceous Makran ophiolite, SE Iran: Monsef *et al.* (2019).

signatures for the studied mafic rocks is generally associated with back-arc basin basalts (Volpe *et al.* 1987; Pearce & Peate, 1995; Pearce & Stern, 2006). A closer look at the REE pattern and trace-element signatures along with trace-element ratios (e.g. Th/Yb, Nb/Yb, Zr/Y, Zr/Ti and Ti/V) of the studied mafic rocks reveal that the Bathani area matches the composition of back-arc supra-subduction zone (SSZ) ophiolitic basalts.

SSZ ophiolites represent oceanic lithosphere formed in the extended upper plates of subduction zones formed by magmatism in the fore-arc and back-arc basin and the nascent stage of arc volcanism, in the region above the Wadati–Benioff zone (Hawkins, 2003). The lavas therefore range from MORB to arc tholeiite to boninite, primarily reflecting formation in different parts of a supra-subduction zone environment (Dilek & Furnes, 2009). The genesis of supra-subduction ophiolites involves subduction initiation, followed by rapid slab rollback leading to extension and seafloor spreading in the downgoing slab. These processes generate melt with MORB-like composition in the proto-arc to back-arc settings during the early phase of melting. In subsequent phases of melting, melt column beneath the proto-arc–back-arc region may be strongly influenced by processes such as slab dehydration and related mantle metasomatism, melting of subduction sediments, repeated episodes of partial melting of metasomatized peridotites and mixing of highly enriched liquids from the deeper fertile source resulting in variable lava composition. Studies by Hawkins (2003) and Dilek & Furnes (2014) have further pointed out that SSZ systems also display rock series ranging from picrites to rhyolites, including arc tholeiitic, high-K calc-alkaline and shoshonitic magma series generated in the associated volcanic arc. Deeper-level arc crust also displays various types of layered and isotropic gabbro as well as granitoid plutons. A wide assortment of sediments ranging from arc-derived tephra and volcanoclastic turbidites to silicic and carbonate oozes also occurs in

https://doi.org/10.1017/S0016756821000078 Published online by Cambridge University Press

SSZ systems. Crustal units are commonly underlain by mafic cumulates and mantle rocks comprising depleted harzburgite, dunite and serpentinized equivalents. The close spatial and temporal association of back-arc basin rocks with arc rocks and volcanic detritus is a significant signature which distinguishes it from MORB ophiolites. The crustal contraction in an SSZ environment would tectonically juxtapose arc, back-arc and fore-arc crust leading to a close spatial and temporal association of back-arc basin rocks with arc rocks and volcanic detritus. This signature distinguishes it as an SSZ ophiolite, differentiating it from MORB-type ophiolites.

We envisage that during juvenile stages of intra-oceanic subduction, a back-arc basin opened up in which basaltic rocks of E-MORB affinity of the CD of Bathani area were generated. This led to a modification of the pre-existing oceanic lithosphere within which subduction started, and in which a magmatic arc formed upon subduction maturation. In this magmatic arc, the mafic and felsic volcanics, andesites and associated pyroclastics were generated. Although the mantle rock sequence pyroxenite-gabbro-anorthosite is not directly exposed in the area, it is preserved as enclaves within the granitoids of the ND. Subduction zone sediment cover is now metamorphosed and manifests itself as clastic sediments, phyllite and quartzite, overlying these units comprising the SD. The 1750–1640 Ma granites/granitoids of arc affinity present in the area cross-cut the ophiolite sequence and, in all probability, mark the post-collisional orogenic events.

Although geochronological records from the massive terrain of the CGGC are limited, Palaeoproterozoic ages corresponding to metamorphic and magmatic events have been reported from different parts of the terrain. Dey *et al.* (2017) reported Late Palaeoproterozoic (*c.* 1650 Ma) ultra-high-temperature metamorphism from the northeastern part of the CGGC, and the *P–T* path inferred by the study supports a convergent margin setting. Saikia *et al.* (2017, 2019) reported Palaeoproterozoic subduction-related felsic magmatism (*c.* 1750–1660 Ma) from the northern part of the terrain. Shreds of evidence of such tectonothermal events from parts of the CGGC establishes beyond doubt its involvement in the evolution of the Greater Indian landmass during the Columbia/Nuna supercontinent assembly. It is significant in the context of our study as the Bathani area is cross-cut by late intruded granites of Palaeoproterozoic age, from which it can be inferred that the mafic rocks precede the granites and have at least a Palaeoproterozoic age. This study and the published petrological, geochemical and geochronological data indicate that the Bathani area is a site of preserved Palaeoproterzoic relics of volcanic back-arc magmas and associated felsic magmatism of arc affinity of subduction regime. The geometrical configuration of the BVSS indicates its emplacement between the Archean to Proterozoic Son-Narmada Lineament zone and the Palaeoproterozoic felsic orthogneisses exposed within the Quaternary alluvium towards the north of the CGGC. Geochemical signatures suggest that the Bathani pillow lavas are reminiscent of Proterozoic supra-subduction zone ophiolite lavas. We compare our data with known occurrences of Proterzoic ophiolitic lavas in India and other geological occurrences, and the similarity is very significant (Fig. 10a–d). We infer that the Bathani mafic pillow lavas and associated chert and dolomites represent the upper part of a supra-subduction-type columnar ophiolite section, which was displaced onto the present-day northern margin of CCGC and is believed to mark the suture between Northern and Southern Indian blocks at *c.* 1.9 Ga.

6. Conclusions

The Bathani–Churi section at the northern fringe of Chotanagpur Granite Gneiss Complex is an exemplary site of well-preserved relicts of a subducted Palaeoproterozoic oceanic crust. It is marked by the presence of pillow basalt and dolerites, intermediate–basic volcanics and associated tuff, chert, jasper and dolomites representing the Bathani volcano-sedimentary sequence. The remnants of the oceanic crust are metamorphosed to low-grade greenschist facies conditions. Fluid mobile elements have therefore been redistributed. However, the fluid immobile elements preserve the primary geochemical signatures. The studied mafic rocks may be the product of MORB-like magma generated by partial melting of the upwelling spinel lherzolite in a back-arc extensional setting. The primary magma corresponds to 4–12% partial melting of spinel lherzolite mantle. Geochemical trends of the Bathani mafic rocks are highly reminiscent of the Proterozoic supra-subduction zone ophiolitic composition. The rock assemblage exposed in the study area implies it is part of the supra-subduction-type ophiolitic section marking the suturing of the Northern and Southern Indian blocks during the Nuna Supercontinent amalgamation during the Palaeoproterozoic Era.

Acknowledgements. The manuscript benefited from insightful, constructive revisions by anonymous reviewers and Editor Dr Kathryn Goodenough. Mansoor Ahmad and Abdul Qayoom Paul express sincere gratitude to the Deputy Director General, State Unit, Bihar for his guidance and encouragement. Mansoor Ahmad express thanks to Additional Director General and Head of Department, North Eastern Region, Shillong, for the manuscript's kind approval for publication. Ashima Saikia acknowledges a Council of Scientific and Industrial Research grant (no. 24(0317)/12/EMR-II).

Supplementary material. To view supplementary material for this article, please visit https://doi.org/10.1017/S0016756821000078

References

Acharyya SK (2003) The Nature of Mesoproterozoic Central Indian tectonic zone with exhumed and reworked older granulites. *Gondwana Research* **6**, 197–214.

Ahmad M and Wanjari N (2009) Volcano-sedimentary sequence in the Munger–Rajgir metasedimentary belt, Gaya district, Bihar. *Indian Journal of Geoscience* **63**, 351–60.

Balaram V, Saxena VK, Manikyamba C and Ramesh SL (1990) Determination of rare earth elements in Japanese rock standards by inductively coupled plasma mass spectrometry. *AtomicSpectroscopy* **11**, 19–23.

Basta FF, Maurice AE, Bakhit BR, Ali KA and Manton WI (2011) Neoproterozoic contaminated MORB of Wadi Ghadir ophiolite, NE Africa: geochemical and Nd and Sr isotopic constraints. *Journal of African Earth Sciences* **59**, 227–42.

Borghini G, Fumagalli P and Rampone E (2010) The stability of plagioclase in the upper mantle: subsolidus experiments on fertile and depleted lherzolite. *Journal of Petrology* **51**, 229–54.

Carlson RW and Ionov DA (2019) Compositional characteristics of the MORB mantle and bulk silicate Earth based on spinel peridotites from the Tariat Region, Mongolia. *Geochimica et Cosmochimica Acta* **257**, 206–23.

Chatterjee N, Banerjee M, Bhattacharya A and Maji AK (2010) Monazite chronology, metamorphism–anatexis and tectonic relevance of the mid-Neoproterozoic Eastern Indian Tectonic Zone. *Precambrian Research* **179**, 99–120.

Chatterjee N, Crowley JL and Ghose NC (2008) Geochronology of the 1.55 Ga Bengal anorthosite and Grenvillian metamorphism in the Chotanagpur gneissic complex, eastern India. *Precambrian Research* **161**, 303–16.

Chatterjee N and Ghose NC (2011) Extensive early Neoproterozoic high-grade metamorphism in North Chotanagpur Gneissic Complex of the Central Indian Tectonic Zone. *Gondwana Research* **20**, 362–79.

Dasgupta S and Sengupta P (2003) Indo-Antarctic correlation: a perspective from the Eastern Ghats Granulite belt, India. In *Proterozoic East Gondwana Supercontinent Assembly and Breakup* (eds M Yoshida, BE Windley and S Dasgupta), pp. 131–43. Geological Society of London, Special Publication no. 206.

Dey A, Karmakar S, Mukherjee S, Sanyal S, Dutta U and Sengupta P (2019) High pressure metamorphism of mafic granulites from the Chotanagpur Granite Gneiss Complex, India: evidence for collisional tectonics during assembly of Rodinia. *Journal of Geodynamics* **129**, 24–43.

Dey A, Mukherjee S, Sanyal S, Ibenz-Mejia M and Sengupta P (2017) Deciphering sedimentary provenance and timing of sedimentation from a suite of metapelites from the Chotanagpur Granite Gneissic complex, India: implications for Proterozoic tectonics in the East-Central part of the Indian shield. In *Sediment Provenance: Influences on Compositional Change from Source to Sink* (eds R. Mazumder), pp. 453–486. Amsterdam: Elsevier.

Dilek Y and Furnes H (2009) Structure and geochemistry of Tethyan ophiolites and their petrogenesis in subduction rollback systems. *Lithos* **113**, 1–20.

Dilek Y and Furnes H (2014) Ophiolites and their origins. *Element* **10**, 93–100.

Elburg MA, Bergen MV, Hoogewerff J, Foden J, Vroon P, Zulkarnain I and Nasution A (2002) Geochemical trends across an arc-continent collision zone: magma sources and slab-wedge transfer processes below the Pantar Strait volcanoes, Indonesia. *Geochimica et Cosmochimica Acta* **66**, 2771–89.

El-Rahman YA, Plot A, Dilek Y, Fryer B, Sharkawy ME and Sakran S (2009) Geochemistry and tectonic evolution of the Neoproterozoic Wadi Ghadir ophiolite, Eastern Desert, Egypt. *Lithos* **113**, 158–78.

Ernst RF (2014) *Large Igneous Provinces*. Cambridge: Cambridge University Press, 641 pp.

Finlow-Bates T and Stumpfl EF (1981) The behaviour of so-called immobile elements in hydrothermally altered rocks associated with volcanogenic submarine exhalative ore deposits. *Mineralium Deposita* **16**, 319–28.

Fitton JG, James D, Kempton PD, Ormerod DS and Leeman WP (1988) The role of lithospheric mantle in the generation of late Cenozoic basic magmas in the western United States. *Journal of Petrology* **1**, 331–49.

Floyd PA and Winchester JA (1975) Magma type and tectonic setting discrimination using immobile elements. *Earth and Planetary Science Letters* **27**, 211–8.

Gribble RF, Stern RJ, Bloomer SH, Stüben D, O'Hearn T and Newman S (1996) MORB mantle and subduction components interact to generate basalts in the Southern Mariana Trough back-arc basin. *Geochimica et Cosmochimica Acta* **60**, 2153–66.

Guo F, Li H, Fan W, Li J, Zhao L, Huang M and Xu WL (2015) Early Jurassic subduction of the Paleo-Pacific Ocean in NE. China: petrologic and geochemical evidence from the Tumen mafic intrusive complex. *Lithos* **224**, 40–60.

Gupta A and Basu A (2000) North Singhbhum Proterozoic mobile belt, eastern India–A review. In *MS Krishnan Centenary Volume*, pp. 195–226. Geological Survey of India, Special Publication no. 55.

Hansen J, Davidson J, Jerram DA, Ottley C and Widdowson M (2019) Contrasting TiO_2 compositions in Early Cenozoic mafic sills of the Faroe Islands: an example of basalt formation from distinct melting regimes. *Earth Science* **8**, 235–67.

Hawkesworth CJ, Turner SP, McDermott F, Peate DW and Van Calstern P (1997) U-Th isotopes in arc magmas: implications for elements transfer from the subducted crust. *Science* **276**, 551–5.

Hawkins JW (2003) Geology of supra-subduction zones—Implications for the origin of ophiolites. In *Ophiolite Concept and the Evolution of Geological Thought* (eds Y Dilek and S Newcomb), pp. 227–68. Boulder, Colorado: Geological Society of America, Special Paper no. 373.

Hirose K and Kushiro I (1993) Partial melting of dry peridotites at high pressures: Determination of compositions of melts segregated from per peridotite using aggregates of diamond. *Earth and Planetary Science Letters* **114**, 477–89.

Hofmann AW (1988) Chemical differentiation of the Earth: the relationship between mantle, continental crust, and oceanic crust. *Earth and Planetary Science Letters* **90**, 297–314.

Hofmann AW, Jochum KP, Seufert M and White WM (1986) Nb and Pb in oceanic basalts: new constraints on mantle evolution. *Earth and Planetary Science Letters* **79**, 1–2.

Hollings P, Smyk M and Consens B (2012) The radiogenic isotope characteristics of dykes and sills associated with the Mesoproterozoic midcontinent rift near Thunder Bay, Ontario, Canada. *Precambrian Research* **214–5**, 269–79.

Humphris SE, Thompson G, Schillin JG and Kingsley RH (1985) Petrological and geochemical variations along the Mid-Atlantic Ridge between 46°S and 32°S: influence of the Tristan da Cunha mantle plume. *Geochimica et Cosmochimica Acta* **49**, 1445–64.

Karmakar S, Bose S, Sarbadhikari AB and Das K (2011) Evolution of granulite enclaves and associated gneisses from Purulia, Chotanagpur Granite Gneiss Complex, India: evidence for 990–940 Ma tectonothermal event(s) at the eastern India cratonic fringe zone. *Journal of Asian Earth Sciences* **41**, 69–88.

Kogiso T, Tatsumi Y and Nakano S (1997) Trace element transport during dehydration processes in the subducted oceanic crust: 1. Experiments and implications for the origin of oceanic island basalts. *Earth and Planetary Science Letters* **148**, 193–205.

Liu B, Chen JF, Ma X, Liu JL, Gong EP, Shi WG and Han BF (2018) Timing of the final closure of the Irtysh-Zaysan Ocean: new insights from the earliest stitching pluton in the northern West Junggar, NW China. *Geological Journal* **53**, 2810–23.

MacDonald R, Hawkesworth C and Heath E (2000) The Lesser Antilles volcanic chain: a study in arc magmatism. *Earth-Science Review* **49**, 1–76.

MacLean WH and Barrett T (1993) Lithogeochemical technique using immobile elements. *Journal of Geochemical Exploration* **48**, 109–33.

Mahadevan TM (2002) *Geology of Bihar and Jharkhand*. Bangalore: Geological Society of India, 563 pp.

Mahato S, Goon S, Bhattacharya A, Mishra, B and Bernhardt HJ (2008) Thermotectonic evolution of the North Singhbhum Mobile Belt (Eastern India): a view from the western part of the belt. *Precambrian Research* **162**, 102–27.

Maji AK, Goon S, Bhattacharya A, Mishra B, Mahato S and Bernhardt HJ (2008) Proterozoic polyphase metamorphism in the Chotanagpur Gneissic Complex (India), and implication for trans-continental Gondwanaland correlation. *Precambrian Research* **162**, 385–402.

McDonough W and Sun SS (1995) The composition of the Earth. *Chemical Geology* **67**, 1050–6.

McKenzie D and O'Nions RK (1991) Partial melt distributions from inversion of rare earth element. *Journal of Petrology* **32**, 1021–91.

Metcalf RV and Shervais JW (2008) Supra subduction-zone ophiolites: Is there really an ophiolite conundrum? In *Ophiolites, Arcs, and Batholiths: A Tribute to Cliff Hopson* (eds JE Wright and JW Shervais), pp. 91–222. Geological Society of America, Special Paper no. 438.

Mohr PA (1987) Crustal contamination in mafic sheets: a summary. In *Mafic Dyke Swarms* (eds HC Halls and WC Fahrig), pp. 75–80. St John's: Geological Association of Canada, Special Publication no. 34.

Monsef I, Rahgoshay M, Pirouz M, Chiaradia M, Gregoire M and Ceuleneer G (2019) The Eastern Makran Ophiolite (SE Iran): evidence for a Late Cretaceous fore-arc oceanic crust. *International Geology Review* **61**, 1313–39.

Montanini A, Tribuzio R and Vernia L (2008) Petrogenesis of basalts and gabbros from an ancient continent ocean transition (External Liguride ophiolites, Northern Italy). *Lithos* **101**, 453–79.

Mukherjee S, Dey A, Sanyal S and Sengupta P (2018) Tectonothermal imprints in a suite of mafic dykes from the Chotanagpur Granite Gneissic complex (CGGC), Jharkhand, India: evidence for late Tonian reworking of an early Tonian continental crust. *Lithos* **320**, 490–514.

Mukherjee S, Dey A, Sanyal S and Sengupta P (2019) Proterozoic crustal evolution of the Chotanagpur Granite Gneissic Complex, Jharkhand-Bihar-West Bengal, India: current status and future prospect. In *Tectonics and Structural Geology: Indian Context* (ed. S Mukherjee), pp. 7–54. Cham: Springer Geology International Publishing AG.

https://doi.org/10.1017/S0016756821000078 Published online by Cambridge University Press

Mukherjee D and Ghose NC (1998) Conglomerate at the base of Bihar Mica Belt metasediments, Koderma district, Bihar and its stratigraphic significance. In *Proceedings of National Seminar on Advancement of Geological Sciences in Bihar* pp. 15–16. Patna: Geological Survey of India.

Mukhopadhyay D (1990) Precambrian plate tectonics in the Eastern Indian Shield. In *Crustal Evolution and Metallogeny* (ed. SPH Sychanthavong), pp. 75–100. New Delhi: Oxford and IBH Publishing Co.

Pearce JA (1996) A users guide to basalt discrimination diagrams. In *Trace Element Geochemistry of Volcanic Rocks: Applications for Massive Sulphide Exploration* (ed. DA Wyman), pp. 79–113. St. John's, Canada: Geological Association of Canada, Short Course Notes no. 12.

Pearce JA (2008) Geochemical fingerprinting of oceanic basalts with applications to the ophiolites classification and the search for Archean oceanic crust. *Lithos* **100**, 14–48.

Pearce JA (2014) Immobile elements fingerprinting of ophiolites. *Elements* **10**, 101–8.

Pearce JA and Norry MJ (1979) Petrogenetic implications of Ti, Zr, Y and Nb variations in volcanic rocks. *Contribution of Mineralogy and Petrology* **69**, 33–47.

Pearce JA and Parkinson IJ (1993) Trace element models for mantle melting: application to volcanic arc petrogenesis. In *Magmatic Processes and Plate Tectonics* (eds HM Prichard, T Alabaster, NBW Harris and CR Neary), pp. 373–403. Geological Society of London, Special Publication no. 76.

Pearce JA and Peate DW (1995) Tectonic implications of the composition of volcanic arc magmas. *Annual Review of Earth and Planetary Sciences* **23**, 281–85.

Pearce JA and Stern RJ (2006) Origin of back-arc basin magmas: trace element and isotope perspectives. In *Back-Arc Spreading Systems; Geological, Biological, Chemical, and Physical Interactions* (eds DM Christie, CR Fisher, SM Lee and S Givens), pp. 63–86. Washington; American Geophysical Union, Geophysical Monograph Series no. 166.

Peltonen P, Kontinen A and Huhma H (1996) Petrology and geochemistry of metabasalts from the 1.95 Ga Jormua Ophiolite, northeastern Finland. *Journal of Petrology* **37**, 1359–83.

Pe-piper G, Matarangas D, Reynolds PH and Chatterjee AK (2003) Shoshonites from Agios Nectarios, Lesbos, Greece: origin by mixing of felsic and mafic magma. *European Journal of Mineralogy* **15**, 117–25.

Polat A, Hofmann AW and Rosing MT (2002) Boninite-like volcanic rocks in the 3.7–3.8 Ga Isua greenstone belt, West Greenland: geochemical evidence for intra-oceanic subduction zone processes in the early Earth. *Chemical Geology* **184**, 231–54.

Pradhan VR, Meert JG, Pandit MK, Kamenov G, Gregory LC and Malone SJ (2009) India's changing place in global Proterozoic reconstructions: a review of geochronologic constraints and Paleomagnetic poles from the Dharwar, Bundelkhand and Marwar Cratons. *Journal of Geodynamics* **50**, 224–42.

Purohit KK, Mukherjee PK, Saini NK, Khanna PP and Rathi MS (2006) Geochemical survey of stream sediments from upper parts of Alaknanda, Mandakini, Bhilangana and Bhagirathi catchments, Garhwal Himalaya. *Himalayan Geology* **27**, 31–9.

Rao CVD and Reddy UBV (2009) Petrological and geochemical characterization of Proterozoic ophiolitic mélange, Nellore–Khammam schist belt, SE India. *Journal of Asian Earth Sciences* **36**, 261–76.

Redman BA and Keays RR (1985) Archaean basic volcanism in the Eastern Goldfields Province, Yilgarn Block, Western Australia. *Precambrian Research* **30**, 113–52.

Rekha S, Upadhyay D, Bhattacharya A, Kooijman E, Goon S, Mahato S and Pant NC (2011) Lithostructural and chronological constraints for tectonic restoration of Proterozoic accretion in the Eastern Indian Precambrian shield. *Precambrian Research* **187**, 313–33.

Robinson JAC and Wood BJ (1998) The depth of the spinel to garnet transition at the peridotite solidus. *Earth and Planetary Science Letters* **164**, 277–84.

Rollinson HR (1993) *Using Geochemical Data: Evaluation, Presentation, Interpretation*. New Jersey: Pearson Prentice Hall, 352 pp.

Rudnick RL and Fountain DM (1995) Nature and composition of the continental crust: a lower crustal perspective. *Reviews of Geophysics* **33**, 267–309.

Rudnick RL and Gao S (2003) Composition of the continental crust. In *Geodesy* (eds RL Rudnick, HD Holland and KK Turekian), pp. 1–64. Oxford: Elsevier, Treatise on Geochemistry no. 3.

Saccani E, Allahyari K, Beccaluva L and Bianchini G (2013a) Geochemistry and petrology of the Kermanshah ophiolites (Iran): implication for the interaction between passive rifting, oceanic accretion, and plume-components in the Southern Neo-Tethys Ocean. *Gondwana Research* **24**, 392–411.

Saccani E, Allahyari K and Rahimzadeh B (2014) Petrology and geochemistry of mafic magmatic rocks from the Sarve-Abad ophiolites (Kurdistan region, Iran): evidence for interaction between MORB-type asthenosphere and OIB-type components in the southern Neo-Tethys Ocean. *Tectonophysics* **621**, 132–47.

Saccani E, Azimzadeh Z, Dilek Y and Jahangiri A (2013b) Geochronology and petrology of the early carboniferous Misho mafic complex (NW Iran), and implications for the melt evolution of Paleo-Tethyan rifting in Western Cimmeria. *Lithos* **16–63**, 264–78.

Saha D, Mazumder R and Kar R (2017) Shallow marine to pelagic sediments from a dismembered ophiolite, Kandra, southern India – glimpses of ancient subduction zone related sedimentation. *Gondwana Research* **49**, 21–41.

Saikia A, Gogoi B, Ahmad M, Kumar R, Kaulina T and Bayanova T (2019) Mineral chemistry, Sr-Nd isotope geochemistry and petrogenesis of the granites of Bathani volcano-sedimentary sequence from the northern fringe of Chotanagpur Granite Gneiss Complex of eastern India. In *Geological Evolution of the Precambrian Indian Shield* (ed. MEA Mondal), pp. 79–120. Bern: Springer Nature, Society of Earth Scientists.

Saikia A, Gogoi B, Kaulina T, Lialina L, Bayanova T and Ahmad M (2017) Geochemical and U–Pb zircon age characterization of granites of the Bathani volcano-sedimentary sequence, Chotanagpur granite gneiss complex, Eastern India: vestiges of the Nuna supercontinent in the Central Indian Tectonic Zone. In *Crustal Evolution of India and Antarctica: The Supercontinent Connection* (eds NC Pant and S Dasgupta), pp. 233–252. Geological Society of London, Special Publication no. 457.

Saini NK, Mukherjee PK, Rathi MS and Khanna PP (2000) Evaluation of energy-dispersive x-ray fluorescence spectrometry in the rapid analysis of silicate rocks using pressed powder pellets. *X-Ray Spectrometry* **29**, 166–72.

Saini NK, Mukherjee PK, Rathi MS, Khanna PP and Purohit KK (1998) A new geochemical reference sample of granite (DG-H) from Dalhousie, Himachal Himalaya. *Journal of Geological Society of India* **52**, 603–6.

Saini NK, Mukherjee PK, Rathi MS, Khanna PP and Purohit KK (2007) A proposed amphibolite reference rock sample (AMH) from Himachal Pradesh. *Journal of Geological Society of India* **69**, 799–802.

Salters VJM and Stracke A (2004) Composition of the depleted mantle. *Geochemistry, Geophysics, Geosystems* **5**, Q05B07.

Sanyal S and Sengupta P (2012) Metamorphic evolution of the Chotangapur Granite Gneiss Complex of the East Indian Shield: current status. In *Paleoproterozoic of India* (eds R Mazumder and D Saha), pp. 117–145. Geological Society of London, Special Publication no. 365.

Sarkar AN (1982) Precambrian tectonic evolution of eastern India: a model of converging microplates. *Tectonophysics* **86**, 363–97.

Sarkar SN and Saha AK (1977) The present status of the Precambrian stratigraphy, tectonics and geochronology of Singhbhum-Keonjhar-Mayurbhanj region, eastern India. *Indian Journal of Earth Science* **4**, 37–65.

Saunders AD, Norry MJ, Tarney J, Pickering KT, Knipe RJ and Dewey JF (1991) Fluid influence on the trace element compositions of subduction zone magmas. In *The Behaviour and Influence of Fluid in Subduction Zones* (eds J Tarney, KT Pickering, RJ Knipe and JF Dewey), pp. 377–392. *Philosophical Transactions of the Royal Society of London, Series A* 335.

Scarrow JH and Cox KG (1995) Basalts generated by decompressive adiabatic melting of a mantle plume: a case study from the Isle of Skye, NW Scotland. *Journal of Petrology* **36**, 3–22.

Shaikh DA, Miyashita S and Matsueda H (2005) The petrological and geochemical characteristics of an ophiolite volcanic suite from the Ghayth area of Oman. *Journal of Mineralogical and Petrological Sciences* **100**, 202–20.

Shaw DW (1970) Trace element fractionation during anatexis. *Geochimica et Cosmochimica Acta* **34**, 237–43.

Shervais JW (1982) Ti-V plots and the petrogenesis of modern and ophiolitic lavas. *Earth and Planetary Science Letters* **59**, 101–18.

https://doi.org/10.1017/S0016756821000078 Published online by Cambridge University Press

Singh Y and Krishna V (2009) Rb–Sr geochronology and petrogenesis of granitoids from the Chotanagpur Granite Gneiss Complex of Raikera–Kunkuri region, central India. *Journal Geological Society of India* **74**, 200–8.

Smith EI, Sánchez A, Walker JD and Wang K (1999) Geochemistry of mafic magmas in the Hurricane volcanic field, Utah: implications for small- and large-scale chemical variability of the lithospheric mantle. *The Journal of Geology* **107**, 433–48.

Spandler C and Pirard C (2013) Element recycling from subducting slabs to arc crust: a review. *Lithos* **170–171**, 208–23.

Sun SS (1980) Lead isotopic study of young volcanic rocks from mid-ocean ridges, ocean island and island arcs. *Philosophical Transactions of the Royal Society of London, Series A* **297**, 409–45.

Sun SS and McDonough WF (1989) Chemical and isotopic systematics of oceanic basalts: implications for mantle composition and process. In *Magmatism in the Ocean Basins* (eds AD Saunders and MJ Norry), pp. 313–45. Geological Society of London, Special Publication no. 42.

Thompson RN and Morrison MA (1998) Asthenospheric and lower-lithospheric mantle contributions to continental extensional magmatism: an example from the British Tertiary Province. *Chemical Geology* **68**, 1–15.

Valsami E and Cann JR (1992) Mobility of rare earth elements in zones of intense hydrothermal alteration in the Pindos ophiolite, Greece. In *Ophiolites and their Modern Oceanic Analogues* (eds LM Parson, BJ Murton and P Browning), pp. 219–32. Geological Society of London, Special Publication no. 60.

Volpe AM, Macdougall JD and Hawkins JW (1987) Mariana Trough Basalt (MTB): trace element and Sr-Nd isotopic evidence for mixing between MORB like and arc like melts. *Earth and Planetary Science Letters* **82**, 241–54.

Watson EB (1982) Basalt contamination by continental crust: some experiments and models. *Contribution to Mineralogy and Petrology* **80**, 73–87.

Weaver BL and Tarney J (1984) Estimating the composition of the continental crust: an empirical approach. *Nature* **310**, 575–7.

Winchester JA and Floyd PA (1977) Geochemical discrimination of different magma series and their differentiation products using immobile elements. *Chemical Geology* **20**, 325–43.

Woodhead JD, Eggins S and Gamble J (1993) High field strength and transition systematics in island arc and back-arc basin basalts: evidence for multiphase melt extraction and a depleted mantle wedge. *Earth Planetary Science Letters* **114**, 491–504.

Woodhead JD, Hergt JM, Davidson JP and Eggins SM (2001) Hafnium isotope evidence for 'conservative' element mobility during subduction zone processes. *Earth and Planetary Science Letters* **192**, 331–46.

Yan Q, Shi X, Metcalfe I, Liu S, Xu T, Kornkanitnan N, Sirichaiseth T, Yuan L, Zhang Y and Zhang H (2018) Hainan mantle plume produced late Cenozoic basaltic rocks in Thailand, Southeast Asia. *Scientific Reports* **8**, 2640.

Zou H and Zindler A (1996) Constraints on the degree of dynamic partial melting and source composition using concentration ratios in magmas. *Geochimica et Cosmochimica Acta* **60**, 711–7.

https://doi.org/10.1017/S0016756821000078 Published online by Cambridge University Press